MODELLING OF MATERIAL REMOVAL IN ELECTROSTREAM DRILLING

A DISSERTATION

Submitted in partial fulfilment of the requirements for the award of the degree of

MASTER OF TECHNOLOGY

in

MECHANICAL ENGINEERING

(With Specialization in Production and Industrial Systems Engineering)

By

AMARENDRAKUMAR BODDU

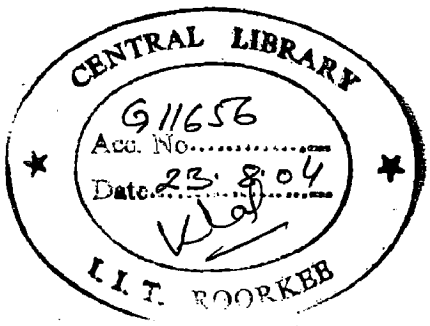

DEPARTMENT OF MECHANICAL AND INDUSTRIAL ENGINEERING
INDIAN INSTITUTE OF TECHNOLOGY ROORKEE
ROORKEE-247 667 (INDIA)

JUNE, 2004

CANDIDATE'S DECLARATION

I here by declare that the work presented in this dissertation entitled **"MODELLING OF MATERIAL REMOVAL IN ELECTROSTREAM DRILLING"** in the partial fulfillment of the requirements of the award of Degree of ***MASTER OF TECHNOLOGY*** in **Production & Industrial Systems Engineering** submitted in ***Department of Mechanical and Industrial Engineering***, Indian Institute of Technology, Roorkee is an authentic record of my own work carried out during the period July 2003 to June 2004 under the supervision of ***Dr. H.S. Shan***, Professor and Head of the department of Mechanical and Industrial Engineering, Indian Institute of Technology Roorkee, Roorkee.

The matter embodied in this dissertation has not been submitted by me for the award of any other degree.

Amarendra Kumar B.
(AMARENDRAKUMAR BODDU)

Date: June 28th, 2004

Place: Roorkee

This is certified that the above statement made by the candidate is correct to the best of my knowledge.

H S Shan 28/6/04
(H.S. Shan)

Professor & Head
Mechanical and Industrial Engineering Department
Indian Institute of Technology Roorkee
Roorkee – 247667

ACKNOWLEDGEMENTS

I take the opportunity to pay my regards and a deep sense of gratitude to my guide **Dr. H.S. Shan,** Professor and Head of the Department of Mechanical and Industrial Engineering, Indian Institute of Technology Roorkee, for his valuable guidance, keen co-operation, and cheerful encouragement throughout my dissertation work.

I wish to express my deep gratitude to **Dr. B.K. Mishra,** Associate Professor, Department of Mechanical & Industrial Engineering, Indian Institute of technology Roorkee for providing valuable tips and support.

I am thankful to Research Scholar **Mr. Mohan Sen** for his instant help in all kinds of work and cooperation through out my dissertation work.

I acknowledge my sincere thanks to **Shri Jasbir Singh and** the other staff of Product Development Lab, Mechanical and Industrial Engineering Department especially for using COMPAQ, Presario, Pentium-4 computer.

I gratefully acknowledge my sincere thanks to all my friends for their inspirational impetus and moral support during the course of this work.

Last but not the least, I wish to place on record my deep sense of gratitude to my **parents** without whose blessings I would not have joined this prestigious department for higher studies to enrich myself with the latest knowledge.

AMARENDRAKUMAR BODDU

ABSTRACT

Electrostream drilling (ESD) process is gaining prominence in the machining of small holes in difficult to machine materials used in space, aviation, electronics and computers, medical, and automobile industries. This process employs a jet of charged acid electrolyte for anodic dissolution of workpiece material. As the trend towards miniaturization continues, this process has shown its superiority over other contemporary non- conventional micro and macro hole drilling processes. The major advantage of this process is to drill small holes having diameter range from 0.125 to 0.2 mm with large aspect ratio.

The present work "Modelling of material removal in Electrostream drilling process" has been completed in two phases. In the first phase we develop a two-dimensional finite element model for the analysis of ESD process using quadrilateral (rectangular) elements. Dimensional analysis has been performed and a relationship between the radial overcut and ESD process parameters has been established. The developed model predicts the overcut and material removal rate.

In the second phase a one dimensional analytical model has been proposed to determine the relationship between the material removal rate and working conditions (Applied voltage, IEG, electrolyte pressure and electrolyte properties), by considering the effect of void fraction alone and later considering the combined effect of electrolyte temperature along with void fraction.

Finally, validation of proposed models has been done with the experimental results and a good correlation between predicted values from proposed models and experimental results has been observed.

NOMENCLATURE

A	Area machined [mm^2]
a_1, a_2, a_3	Constants
b_1, b_2, b_3	Constants
C_c	Concentration of electrolyte
C_p	Specific heat of electrolyte $[KJ/Kg^0C]$
c_1, c_2, c_3	Constants
D	Nozzle diameter [mm]
d_{entry}	Hole entry diameter [mm]
E	Electrochemical equivalent of the work material [kg/coulomb]
E_v	Effective voltage [Volts]
F	Faraday's constant [Coulomb]
f	Feed rate [mm/min]
h	Inter-electrode gap [mm]
I	Current flowing through Inter-electrode gap [Ampere]
i_a	Current density at anode [A/mm^2]
IEG	Inter-electrode gap [mm]
J	Jacobian matrix
k	Electrolyte conductivity [$\Omega^{-1}mm^{-1}$]
k_0	Electrolyte conductivity at temperature T_0
k^1	Constant
M	Mass of ions dissolved [gm]
MRR	Material removal rate (mm/min)
m	Constant
N	Atomic weight of the metal [g/mole]
N^e	Interpolation function
n	Valency of the metal

n^1	Unit normal of anode surface
P	Inlet electrolyte pressure [N/mm^2]
Q	Volumetric metal removal rate [mm^3/min]
Q_l	Electrolyte flow rate [l/min]
R_{0c}	Radial overcut [mm]
R_g	Gas constant
r_c	Corner radius of the tool [mm]
S^m	Stiffness matrix
S_{ij}	Coefficients of stiffness matrix
T	Temperature of electrolyte $\left[^0C \text{ or } K\right]$
u	Electrical potential [Volt]
u^e	Column vector
V	Applied voltage (Volts)
v	Electrolyte flow velocity [m/sec]
w_i	Weighing function
x_0	% Composition of element
x	Distance along electrolyte flow direction [mm] or (x-coordinate)
y	Co ordinate measured in y-direction
ρ_m	Density of work material [kg/m^3]
ρ_e	Density of electrolyte [kg/m^3]
α_t	Temperature coefficient of electrical conductivity of the electrolyte [/k]
α_{vf}	Void fraction
α, β	Constants
δ	A ratio of gas volume to liquid volume
θ	Increase in temperature [k]
η	Current efficiency of anodic dissolution
ϕ_i	Residue

(ξ, η)	Co-ordinates in local system

Subscripts

e	Electrolyte, equilibrium
FE	Finite element
g	Gas
i, j, k....s	Node numbers
l	liquid
m	Work material
o	Initial condition
oc	Overcut

Superscripts

e	Elements
T	Transpose of a matrix
1,2..etc	Element number

CONTENTS

LIST OF FIGURES

LIST OF TABLES

CHAPTER 1

INTRODUCTION

1.1 Introduction

With the recent advancement of technology more and more challenging problems are faced by the scientists and technologists in the field of manufacturing. Three principal types of requirements demanded by the present manufacturing industries are versatility, accuracy and productivity. Thus, there is a need for manufacturing processes that are more readily and accurately controlled and can machine readily even the most difficult to machine materials such as super alloys to intricate and accurate shapes. High tool wear and excessive heat generation are encountered with the conventional machining techniques while machining these materials. For these reasons, alternatives to traditional machining techniques are sought and developed over the last two decades [6,12]. So, non-traditional machining processes are preferred as a better alternative for machining difficult to machine materials.

The notable non-traditional machining processes in this field are: electrochemical machining (ECM), electro discharge machining (EDM), electron beam machining (EBM), laser beam machining (LBM), ultrasonic machining (USM), plasma arc machining (PAM) etc. These processes are now used commercially in different walks of life. Out of these, electrochemical machining (ECM) has shown the greatest potential for satisfying the needs of the present manufacturing industries [4].

There was an opinion that as metals can be electro-deposited from aqueous solutions, it should be possible to dissolve them electrolytically. Possibly because cathodic behavior of metals had attracted far more attention than their anodic behavior, the latter having been regarded mainly as an essential constant of electro deposition and not otherwise as of practical interest. No serious efforts were made to take advantage of anodic dissolution specifically as a means of removing metal.

In 1929, the first application of electrolysis for metal removal was proposed when a Russian, W. Gosseff filed a patent for an electrochemical machining process. A very little interest was shown in this process at that time, because materials at the time could easily be drilled or machined by conventional methods as the difficult-to-machine

materials had not developed at that time. In the last few decades the use of ECM and its associate processes have shown rising trend in the manufacturing industries due to the ever-increasing demand for the use of difficult to machine materials [25,26].

1.2 Electrochemical Machining

ECM is a non-traditional machining process in which a shaped tool or electrode is used to remove material from the workpiece. Here the tool as a cathode and workpiece as anode are connected to the DC power source to maintain the high current densities between the tool and workpiece (Fig 1.1). An electrolyte is pumped through the small gap, which is maintained between the tool and workpiece. The chemical properties of electrolyte are such that the constituents of the work material go into the solution by the electrolytic process [36].

In ECM, either the tool remains stationary during the process and as machining proceeds the gap widens or the tool is fed towards the workpiece such that the feed rate exactly matches the erosion rate on the work surface [13].

The main advantages of ECM [36] are as follows:

(a) The rate of metal machining does not depend on the hardness of the metal,

(b) Ability to machine complex three-dimensional curved surfaces without the striation marks,

(c) No tool wear,

(d) Stress-free machined surface with high surface finish.

1.3 Complex Nature of the ECM Process

The basic equation for the computation of the metal removed in ECM operation is derived from Faraday's law of electrolysis.

$$M = \frac{EIt}{F} \tag{1.1}$$

This equation is based on a number of simplified assumptions such as

1. Metal dissolution efficiency is constant and equal to 100%,
2. Valency of the work material being machined remains constant throughout machining,
3. The electrolyte properties are uniform over the entire working area and do not change with time,

4. Effect of the presence of the gases evolved during the process during machining is negligible,
5. The over-potential on the surfaces of the electrodes is negligible.

When the anode is made of an alloy instead a pure metal, the volume of alloy removed per unit charge [12] can be estimated as

$$Q = \frac{100}{\rho_m F}\left(\frac{1}{\sum_i x_{0i} n_i / N_i}\right) \tag{1.2}$$

1.4 Parameters affecting Metal Removal in ECM

The process variables that influence the rate of electrochemical dissolution and surface generation in ECM have been discussed by Rourke and Kennedy [33]. These are voltage, electrolyte viscosity, electrolyte pressure, electrolyte temperature, electrolyte velocity, feed rate, current distribution, electrolyte contamination, work material and tool material.

The stock removal equation in ECM is based on a number of simplified assumptions and does not account for the effects of some significant factors. Therefore it cannot be expected to yield accurate results under actual working conditions. These process variables are change in valency of electrochemical dissolution during the operation, gas evolution and bubble formation, and electrolyte conductivity during the process [18].

1.4.1 Valency of Electrochemical Dissolution

In ECM, work material would not necessarily dissolve at a constant valency throughout. For example, dissolution of iron in NaCl solution may be either in the form of ferrous hydroxide (Fe^{2+}) or ferric hydroxide (Fe^{3+}) depending upon the machining conditions. Copper in chloride solution can dissolve in mona-valent state where as, in nitrate solutions it can be assumed in divalent form [10]. In machining of steel dissolution has been found to occur at alternative valency combinations of $Fe^{3+}Cr^{6+}$ or $Fe^{2+}Cr^{3+}$. Mode of dissolution while machining complex alloys is still more difficult to analyze. In the majority of cases, the preferential valency mode of dissolution has been found to depend upon the electrolyte flow rate, inter-electrode gap and metal removal rate. Incorrect assumption regarding the valency of dissolution can often lead to current

efficiency values of more than 100% thus introducing appreciable amount of error in the values computed from equation (1.1) [18].

1.4.2 Gas Evolution and Bubble formation

During electrochemical dissolution gases like hydrogen and oxygen are evolved. Equations given below show the evolution of these gases. The evolution of gases leads to low dissolution efficiency at reduced current density.

Two kinds of reactions occur at the cathode; they are plating of metal ions and evolution of hydrogen gases are described below.

Metal plating:

$$M^{+} + e^{-1} \rightarrow M \text{ (M is any metal)} \tag{1.3}$$

Hydrogen gas evolution:

$$2H^{+} + 2e^{-1} \rightarrow H_2 \uparrow \text{ (in acid solution)} \tag{1.4}$$

$$2H_2O + 2e^{-1} \rightarrow 2(OH)^{-} + H_2 \uparrow \text{ (in alakaline solution)} \tag{1.5}$$

Under the given conditions whether plating or hydrogen gas evolution will take place is governed by electrode potential.

Similarly, two kinds of reactions take place at the anode; they are metal ion dissolution and oxygen gas evolution, as follows

Metal dissolution:

$$M \rightarrow M^{+} + e^{-} \text{ (acidic solution)} \tag{1.6}$$

$$M^{+} + (OH)^{-} \rightarrow MOH + e^{-} \text{ (in base solution)} \tag{1.7}$$

Oxygen evolution:

$$2H_2O \rightarrow O_2 \uparrow + 4H^{+} + 2e^{-} \text{ (in acid solution)} \tag{1.8}$$

$$4(OH)^{-} \rightarrow 2H_2O + O_2 \uparrow + 4e^{-} \text{ (in alkaline solution)} \tag{1.9}$$

Since part of the current through cell is associated with oxygen evolution at the work surface and therefore, current efficiency is normally below 100% [18].

1.4.3 Electrolyte conductivity

Electrolyte conductivity (K) is determined by the type and number of ions present in the electrolyte and their mobility. It is a function of electrolyte temperature and it is represented by equation (1.10). Normally, the temperature distribution obtained in inter-electrode gap is non linear. The value of temperature coefficient of electrolyte

conductivity varies but for simplification, in majority of the models, it has been assumed to be constant.

$$K = K_0(1+\alpha_t\theta) \tag{1.10}$$

Another important factor in the determination of electrolyte conductivity is the void fraction (it is the ratio of the volume taken by voids to the total volume of a material). It was reported that void fraction and temperature effects are of the same order of magnitude and the expression for electrolyte conductivity by considering the effect of void fraction [15] as follows

$$K = K_0(1+\alpha_t\theta)(1-\alpha_{vf})^m \tag{1.11}$$

In the above equation (1.11) the value of m was 1.5 for the case of uniform void distribution. Where as for non-uniform distribution its value was taken as 2 when bubbles are concentrated near the cathode. Experimentally the void fraction (α_{vf}) [19] can be evaluated from equation (1.12)

$$\alpha_{vf} = \frac{\delta}{1+\delta} \tag{1.12}$$

From equation (1.11) it can be seen that the electrolyte conductivity is proportional to the electrolyte temperature and inverse of the void fraction. The increase in the electrolyte temperature along the stream tends to raise its conductivity, but the increase in the void fraction along the stream tends to reduce the electrolyte conductivity. However, the effect of void fraction on the electrolyte conductivity is more than that of temperature. Hence, electrolyte conductivity decreases along the flow path [15].

ECM has found wide range applications in a number of practical machining operations such as turning, grinding, deburring, broaching, trepanning, honing and fine hole drilling. Some of the typical examples of ECM applications are: machining of turbine blades, cutting curvilinear slots, machining intricate patterns, production of long curved profiles, machining of gears and production of integrally bladed nozzle-rings for use in diesel locomotives [6].

ECM based methods such as electrochemical drilling (ECD), shaped tube electrolytic machining (STEM), capillary drilling (CD), electrostream drilling (ESD) and electro jet drilling (EJD) have emerged as the most appropriate methods for drilling small holes in difficult-to-machine to materials.

In Electrochemical Drilling (ECD) a tubular electrode is used as cathode tool (mostly made of titanium). It moves gradually into the electrically conductive workpiece, which acts as anode. Electrolyte is pumped down the central bore of tool, and out through the side gap formed between the wall of the tool and the hole. The main machining action is carried out in the inner electrode gap formed between the leading edge of the tool and the base of the hole in the workpiece. Out side of the electrode is covered with insulating coating to protect the electrode from the acid attack [27].

In Capillary Drilling (CD), a fine glass capillary with very fine (such as platinum) wire is used as cathode and electrolyte is passed down the glass tube to the machining area. As the path of electrolyte is shorter in CD, there is less resistance, and the resistive path of current flow must be overcome by a lower operating voltage (100V-200V). CD is mainly used in trailing edge holes in high-pressure turbine blades in the range of 0.2 to 0.5 mm to a depth of about 8 to 16 mm [22].

Shaped Tube Electrolytic Machining (STEM) is a non-contact electrochemical drilling process for drilling high aspect ratio holes. The tool is a hollow shaped titanium tube, which acts as a cathode and conductive workpiece as anode. The electrode is covered with a thin, organic coating on all its exterior surfaces except at the tip and carefully straightened and guided into the work piece material. The cutting tip of the electrode is exposed bare. This ensures that machining occurs only at the tip of the electrode and not along its length. STEM uses acid electrolyte that is fed through the tube to the tip and returns along the outside of the coated tube to the top of the workpiece [2].

In Electrostream Drilling (ESD) a jet of acid electrolyte from glass tube nozzle under pressure (0.3-1.0 N/mm^2) is made to impinge on the workpiece to achieve the anodic dissolution of the work material. The electrolyte gets charged when a platinum wire inserted into the glass nozzle is connected to the negative terminal of DC power supply. The workpiece acts as anode, when a suitable electric potential is applied across the two electrodes, and the charged electrolyte stream strikes the workpiece. The material removal takes place through electrolytic dissolution. The metal ions thus removed are carried away with the flow of electrolyte. In ESD high working voltage upto 500V (DC) and electrolytes of high conductivity are used in order to obtain high current density required for achieving a high anodic dissolution rate. The major advantage of

electrostream drilling process is its capability to drill holes in the diameter range of 0.125 mm to 0.2 mm [5,6].

Electrojet Drilling (EJD) differs from the previous techniques in not requiring the entry of capillary into the workpiece. The jet of electrolyte itself causes the dissolution and room is required for electrolyte to return preferably in the form of spray. The electrolyte jet is formed by a nozzle drawn glass tube for the required size of hole. The holes produced by electrolyte jet greatly depend on the throwing power of the electrolyte and the pressure of the electrolyte. High working voltages and electrolytes of high conductivity are used in order to obtain the high current density required for achieving a high anodic dissolution rate [29]. The specifications of the acid based drilling processes are shown in the Table 1.

CHAPTER 2

ELECTROSTREAM DRILLING (ESD)

2.1 Introduction

Electrostream drilling (ESD) is a special version of electro chemical machining adapted for drilling small holes (usually less than 1mm) by using high voltages and acid electrolytes. ESD was first developed in the mid 1960s by the General Electric Company, Aircraft Engine Group. The process was invented to solve the problems associated with drilling thousand of small cooling holes in turbine blades [2].

ESD uses acid electrolyte instead of the salt electrolytes normally used in ECM to drill small holes. The use of acid electrolytes ensures that the metal sludge by-products from the electrolytic deplating are dissolved and carried away as metal ions. This eliminates clogging of the electrolyte flow around the electrode [6].

The nozzle and electrically conductive workpiece are connected to negative and positive terminal of the DC power supply. As the charged electrolyte stream impinges on the workpiece, material is removed through the electrolytic dissolution and is flushed from the machining area in the form of metal ions in solution. ESD process is effective for drilling brittle or difficult-to-machine metals with small holes at steep angles or curved surfaces [22].

Two different ESD techniques are currently used depending upon the requirements of the application. They are known as penetration drilling and dwell drilling. Penetration drilling is used when deep and accurate holes are required and a nozzle in-feed system is available. The drilling cycle for the penetration technique begins when the nozzle is rapidly fed towards the workpiece but with a reduce charging current in the system. A gap-sensing device monitors the current, slow the feed, and triggers full power when the proper nozzle-workpiece gap is detected. During the drilling cycle, the nozzle is fed in to the hole at a constant feed rate to maintain a constant gap through out the drilling cycle [6].

Dwelling technique is used when shallow, less accurate holes are required or when machine capabilities or workpiece configuration cannot support a nozzle in feed mechanism. In dwell drilling, fixing the nozzle at the proper gap distance from the work

surface and performing the drilling sequence with out nozzle feed. In this technique, the tip of the nozzle never penetrates into the workpiece, the relatively coherent stream of charged jet is solely responsible for determining both the shape and diameter of the hole. This technique eliminates the need for tool-feed and gap-sensing equipment, it also limits the depth and accuracy capabilities of the process.

Two concepts are generally used for charging the acid electrolyte. They differ in the charging electrode that consists of either a metallic sleeve or a small titanium wire, which is placed inside the large diameter section of the ES nozzle as close to the throat as possible [6].

2.2 Equipment and Tooling

Electrostream drilling is a high voltage process in which a voltage is applied between the workpiece and a cathode wire usually made of titanium placed in glass nozzle (Fig 2.1). The voltage (250-650 V) applied drives the current through an electrolyte column.

This process also requires an extra tank in the electrolyte system. The acid electrolyte is pumped from one tank and, after traveling through the machine, overflows into a separate tank, which is electrically insulated from the first. Thus the current is prevented from making complete circuit around the system. It is important that Electrostream drilling machine must be grounded and guarded to prevent voltage mishaps.

Electrostream drilling uses a nozzle shaped glass tube as a cathode. A platinum wire is inserted in the tube to give supply to the acid electrolyte. Electrostream drilling machines have one feed axis capable of producing constant feed rates between 0.125 to 0.25 mm/min as well as jogging movement. Multi axis machine units allow rotation of the part or allow an array of tubes to be indexed across the part. Feed rates and voltages are programmed by using a computer numerical control [2].

2.3 Power Supply

The power supply used for Electrostream drilling is full wave rectified, D.C power supply. The supply can be designed to have a multi channel output if required, each channel feeding a separate manifold.

2.4 Electrolyte System

For electro stream drilling, double electrolyte system is used (as discussed above). The electrolyte system must be environmentally secure, and all relevant regulation must be considered. A line break in the electrolyte system pipe work can cause acid to be thrown out under pressure. The system should be grounded and guarded against all such accidents. The following are the sub systems of electrolyte system

- A recirculating pump
- Filters
- Temperature controller
- Acid mixing facility
- Waste acid disposal facility

In addition, electrolyte concentration and metal contamination monitoring devices are desirable (but not essential). However, it is necessary to have some device to measure acid concentration. Metal contamination should be determined based on the volume of metal removed by drilling, so that acid can be discarded at a predetermined point. The maximum limit of metal contamination is about 3 g/l, depending on the workpiece being drilled [2,6].

2.5 Workpiece Holding Fixtures

Fixtures should be made of materials least affected by acid electrolytes. Perspex or commercially pure titanium may be used for this. They can have carbide-locating points, but these will have to be replaced regularly. It must be remembered that the tool has to transfer current into the workpiece and that any restriction relative to this must be curtailed [2].

2.6 Cathode Holders

These are built so that the cathode is parallel to the feed axis of the machine. Many stations can be placed in one machine, each station will be used to drill at all or some of the holes depending upon the holes spacing and the minimum possible tube spacing. If the glass tubes can not be held close enough together to drill holes simultaneously in one piece, the workpiece will have to be passed through each station until all the holes are drilled [2].

2.7 Glass nozzles

Glass tube 3 or 8 mm in diameter, with the front drawn to the necessary cutting tube size of 0.15 to 0.60 mm is used. The length of this small-diameter section of the tube is responsible to drill the hole. The importance of accurate tubes cannot be overemphasized. The tips must be lapped flat with no chip or crack. The concentricity of the outside and inside diameter is critical. The inside diameter must be kept free of obstruction at all times. [2,6]

2.8 Process Parameters

The key process parameters for ESD include [2]

Voltage: 250 to 650V

Electrolyte: type: a). Type: acid: Sulphuric acid, nitric acid or hydrochloric acid

b). Concentration of 15 to 50% by volume

c). Pressure: 0.275 to 0.40 N/mm^2

d). Temperature: 40°C for sulphuric acid and 20°C for others

Feed rate: 0.75 to 2.5mm/min.

2.9 Process Capabilities

2.9.1 Material removal rates and tolerances

Penetration rates 1.5 to 3.0 mm/min are typical for the super alloys. The electrolytic dissolution follows Faraday's law and current density is limited by the boiling of electrolyte in the nozzle from the resistive heating. Diameter tolerances are typically +/- 0.025 mm or plus or minus 5 percent for sizes above 0.5mm.

2.9.2 Surface roughness

Surface roughness in the holes ranges from 0.4 to 1.6 μm R_a. There are no metallurgical changes when the electrolyte and operating parameters are compatible with the metallurgical state of the workpiece. The holes produced by this process are free from the induced residual stress. Thermal damage is nonexistent. [2]

2.10 Advantages

The advantages of electrostream drilling include the following [2,6]

- No heat-affected zone.
- No burrs are produced.
- No induced stress in the workpiece.

- Not affected by the hardness of the metal.
- Blind and intersecting holes can be drilled.
- No recast layer.

2.11 Limitations

Electro stream drilling can be used only on corrosion resistant metals (stainless st cobalt, and nickel base turbine engine alloys) and electrically conductive workpi Generally this process can not drill commercially pure titanium and refractory met Other limitations are [2,6]

- Process is slow when drilling single hole.
- Expensive electrodes.
- Handling of acid requires special workplace and environmental precautions.
- Chances of nozzle breakage since glass is a fragile material.
- Bell-mouth hole entrance.
- High preventive maintenance cost.

2.12 Applications

Applications of electrostram drilling include [2,6]

- Drilling rows of cooling holes in gas turbine blades and vanes.
- Machining of oil passages.
- Machining of fuel nozzles.
- Starting holes for wire EDM cuts, especially where the length of cut exceeds mm.
- Drilling oil passages in bearings in which EDM will cause cracks.
- Drilling regular arrays of holes in corrosion resistant metals of low machinab (for example, strainers and dies).

CHAPTER 3

LITERATURE REVIEW

Electrochemical machining process and its associate processes are used for diversified precision machining allocations and making holes in turbine blades, finishing dies etc. The mechanism of the ECM and its allied processes is quite complex. The majority of the available literature belongs to the parametric optimization and tool design problems in ECM. Limited research papers are available on other ECM based processes such as Shaped Tube Electrolytic Machining (STEM), Capillary Drilling (CD), Electrojet Drilling (EJD) and Electrostream Drilling (ESD). The available literature on these processes only provides the qualitative aspects of these processes.

Chryssolouris and Wollowitz [9] proposed a new hole making technique to overcome problems facing with the insulated tool. Uninsulated tool and $NaClO_3$ as an electrolyte was used in the technique. This technique was used to produce a large number of small holes in stainless steel plates. This technique is based upon the principle that if machining parameters were carefully controlled it might be possible to use a passivating electrolyte to make holes with un-insulated tools.

A transpassive condition would exist at small front gap while passive conditions are obtained along the side of the holes. Thus the hole width would increase much more slowly than its length. Some taper would probably result, but this could be controlled by adjusting the parameters. The surface quality along the sides of the holes would be acceptable if a passivating electrode is used. However, if additional finish is needed, the uninsulated tool would remain in the hole and an increase of applied voltage would raise the hole walls to a transpassive condition.

Newton [2] points out the difficulties in using alkali salt solution as electrolytes in some applications especially in the case of small holes. While drilling these types of holes, the electrolyte layer between the electrodes is very fine and since the tool is very small in diameter, large current densities are encountered. Due to current density the salt solutions (e.g. NaCl) precipitates in gap that retard the progress of machining.

Strong acid electrolytes like sulphric acid, hydrochloric and nitric are used to overcome the precipitation problem.

Newton [2] used shaped tube electrolytic machining with acid electrolyte. Hollow shaped tube made of pure titanium coated with a special resin for electrical insulation used as cathode with the front (drilling face) lapped flat. Here the straightness of the cathode is critical one. Electrolyte is pumped to machining area through hollow tube cathode. The insulation on the side-walls of the tube prevents the corrosion attack of the acid electrolyte. Generally the process is limited to drilling holes in stainless steel and other corrosion resistant metals and alloys due to the use of an acid electrolyte.

According to **Wilson [37]** the flow rate of electrolyte is quite important in ECM hole making. Because the electrolyte must adequately remove the heat and the product of chemical reaction, flow can be related to the amount of current used. Larger the ratios of flow to current used, better the removal of heat and reaction product. However, the cost of pumping increases as the flow increases, and excessive flow rate can cause local erosion on the workpiece or the tool.

Jain and Pandey [20] developed a two-dimensional model based on the finite element technique for analyzing ECM process using simplex triangular elements. This model has been used to predict the metal removal, current density, and temperature and anode profile. The developed FET-22 model helps in achieving an accurate tooling design in ECM.

Rama Rao and Mishra [29] developed a theoretical model for determining the metal removal in case of electro jet drilling process. It was concluded that with the increase in voltage the current efficiency decreases and the material removal rate is high at higher flow discharge condition.

Hardisty et. al. [13] used the FEM (Finite Element Method) to simulate the ECM process. The FEM was used to determine the two-dimensional potential and flux distributions in the electrolyte, in order to estimate surface erosion. The complex distributions produced in the electrolyte have yielded considerable insight into the erosion process for the tool shapes used in practice.

Chang and Hourng [15] used a body-fitted transformation to predict precisely the gradient of the electrical potential field, and a bubbly-two-phase model was used to simulate the quasi-static electrochemical drilling process. Finally they concluded that the electrolyte conductivity as well as the electrode gap are affected by the void fraction, but not by the electrolyte temperature. The overcut was reduced by using a side coated tool. Metal removal rate and the machining efficiency can be enhanced by increasing the electrolyte flow flux. The increase in the tool feed rate increases the void fraction and reduces the electrolyte conductivity, this results in a decrease in the workpiece overcut.

Hourng and Chang [16] used a theoretical model to simulate the transport properties of electrochemical drilling. Results have shown that transport properties such as velocity, pressure, etc., vary abruptly in the transition region. In the transition region, the electrolyte pressure is higher near the workpiece than near the tool. However, the rate of change of pressure in the stream-wise direction is lower near the workpiece than near the tool in the transition region. A high tool feed rate and a low applied voltage is desired to increase the accuracy of an electrochemical drilling (ECD) process. 2% difference in the prediction of the workpiece overcut was reported as the influence of the flow and thermal fields was included or excluded.

Kozak et. al. [22] developed a one dimensional and two-dimensional mathematical models for determining the machining rate and working conditions like applied voltage, IEG, electrolyte jet velocity and electrolyte properties of Electrochemical jet machining (ECJM). This model describes a distribution of electric field and the effect of change of conductivity of electrolyte on the process performance.

Kozak et. al. [21] developed a mathematical model to determine the material removal and other process parameters using a universal tool electrode of simple shape with complex, controlled kinematics along the workpiece.

Noot et. al. [27] developed a mathematical model to determine the effect of parameter variations on the shape of the turbulators (in order to increase the heat transfer in the turbine blade holes, the wall of the cooling passage is provided with multiple ribs and these irregularities are termed as turbulators) in electrochemical drilling (ECD). They

further used this model for computer simulation. By using the Finite element method (FEM) the dissolving rate of metal was computed.

Chang et. al. [8] used a numerical method to predict a tool shape for a required workpiece shape in electrochemical machining. It was proved that the relative error of the corresponding workpiece in the present calculations can be reduced to about 0.002 when proper machining conditions and numerical parameters were chosen. The effect of the thermal-fluid properties should be considered in the inverse problem, and they conclude that the void fraction is the most important factor in determining the electrolyte conductivity.

Ruszaj and Zybura [30] developed a mathematical model for electrochemical machining with universal rectangular electrode moving above the machined surface and they proposed a relationship for calculating the material removal rate. It was concluded that, with voltage increases metal removal rate increases because of the increase in the intensity of dissolution process.

Hocheng et. al. [14] presented a theoretical and computational model to illustrate how the machined profile evolves as the time elapses. The analysis was based on the fundamental law of electrolysis and the integral of a finite-width tool. The influence of experimental variables including time of electrolysis, voltage, molar concentration of electrolyte and electrode gap upon the amount of material removal and diameter of machined hole was presented and concluded that the time of electrolysis is the most influential factor on the produced diameter of hole.

Gaikwad et. al. [11] made an attempt to predict the profile and size of the work surface generated in micro-ECM process using finite element method. It was concluded that the resulting work profile obtained is a function of current density, current efficiency and time.

There is no published literature is available about the process modelling and optimization except the qualitative description of the process and its applications [1,3-5,29,35]. The effect of process parameters on the process performance is not completely known. No effort seems to have been made toward modelling and optimization of the

process. The present work describes the use of finite element method using Galerkir approach for the ESD process analysis. Further analytical modelling is done to establi the relationship between major process parameters.

Objective of the Present Work

One of the serious problems faced by ESD user industries is the precise control the process. The analytical analysis and an optimizing model of the process are requi for exercising the effective control on the process. Therefore, the work embodied in t dissertation has been aimed towards

1. To develop a two-dimensional finite element model for the analysis of the E process for predicting the material removal rate by considering the effects electrolyte concentration and temperature on electrolyte conductivity.
2. To evaluate the overcut analytically, by developing a new working equation t is simple and economical to use, by employing the dimensional anal technique.
3. To develop a one dimensional analytical model for determining the relation between the response parameter and the process variables like applied volt electrolyte jet flow velocity, inter-electrode gap and electrolyte properties considering the effect of (a) void fraction and (b) void fraction and electrc temperature.
4. To validate the proposed models from the adapted experimental data.

CHAPTER 4

ECM MODELLING PROCEDURES: AN OVERVIEW

The classical theory of ECM is valid under ideal conditions only. An alternative method to obtain the anode shape is to calculate the working gap. With the availability of high speed computers it is now possible to determine the workpiece geometry by successive approximations. Since the computing time is only a fraction of that required for carrying out the experiments, analytical models have proved to be time saving and economical. A number of models have been developed, to predict the work shape obtained in ECM [19]. They are

4.1 $\cos\theta$ Method

This method is based on the computation of equilibrium gap, h, for the given conditions but excludes the consideration of mode of electrolyte flow, over-potential, electrolyte conductivity, heat transferred to the environment etc. In this method, equilibrium work shape is computed corresponding to the tool whose profile has to be approximated by a large number of planar sections at different angles.

The scope of this method is limited to

1. Regions with sharp corners cannot be analyzed. Generally applicable only for $\theta \leq 45$,
2. It is not possible to account for the effects of the mode of electrolyte flow, void fraction, change in electrolyte temperature and conductivity, heat conducted away to the tool and work, etc.

Researchers have also expressed conflicting opinions about the reference surface for the measurement of the angle θ. In view of the approximations involved this method is not recommended for complex shaped workpiece.

4.2 Finite Difference Method

The $\cos\theta$ method is based on the assumption that the lines of electric potential are straight and normal to the electrode surfaces, but this is not true when electrodes with small radii are used. In such cases, it is necessary to know the electrical potential distribution in order to determine the current density, material removal rate, transient and

equilibrium anode profile etc. The Finite difference method (FDM) has been employed specially for the case of non-passivating electrolyte with constant conductivity and temperature. In such cases electric field flow lines are governed by Laplace's equation along with the boundary conditions.

Backward differences or central differences technique is used to solve a set of simultaneous equations obtained from Laplace's equation after imposing the boundary conditions. Corresponding to the potential distribution obtained, the instantaneous current density at the anode surface can be evaluated.

Fig 4.1 shows the tool-work surfaces and IEG drawn in square mesh. The initial potentials at the grid points within the IEG region are set by linear interpolation along the vertical grid lines between the tool and work boundaries. For a point 'o' located in a of spacing mesh h (i, j) we can write

$$u_{ij} = \left(u_{i+1,j} + u_{i-1,j} + u_{i,j+1} + u_{i,j-1}\right)/4 \tag{4.1}$$

equation (4.1) shows that the potential at any point u (i,j) on the square mesh is equal to the mean of the potentials at the four nearest adjacent points (i.e., 1,2,3 and 4 in Fig 4.1). The procedure of computation in this case is to consider each grid point (i,j) within the field and adjust its potential value to the mean of those at the four points around it and to repeat the process until the potential values attained are correct within the prescribed tolerances. The work and tool boundaries are fixed at known potential and therefore, their values are not adjusted during the relaxation process. In few cases, all the points on the tool and work boundary may not lie on grid points (Fig 4.1) and the regular stars may not be formed, such problems can be attempted by the use of over relaxation technique. To solve such type of problems, it was suggested to the use of irregular grids along with regular grids. In this case, a polynomial equation can be used instead of a linear interpolation equation to describe the potential distribution in the area around a nodal point including its near neighbors.

$$u = B_1x^2 + B_2y^2 + B_3x + B_4y + B_5 \tag{4.2}$$

After each computational interval of Δts, work and tool boundaries are moved to new locations, according to the cut and feed vector. For simplicity, consider only the vertical component of the cut vector, which is proportional to the vertical potential gradient at the

work boundary. However, for precision in the results, movement of the cut vector in both x and y directions should be considered.

It is thus evident that FDM would yield approximate results. Further, in case of complex shaped IEG, the tool work boundaries cannot be matched accurately using square meshes, which introduces still greater approximations. On account of approximations involved in use of this method, the authors recommended the use of FEM as it is a better method for the prediction of anode profiles.

4.3 Analogue Method

Laplace equation was first solved by the conducting paper analogue. In this case, equipotential surfaces representing the anode and cathode, to an approximate scale, have to be drawn on a conducting paper. The work surface is segmented to evaluate local current density and then it is moved to the position they would occupy at the end of the time interval Δt. This could be obtained by finding point-to-point movement by the vectorial addition of feed rate vector $\left(f_f \Delta t \cos\theta\right)$ and cut vector $\left(k\frac{\partial \phi}{\partial n}\Delta t\right)$. The method is based on the assumption that feed rate velocity and cut velocities are constant over the time Δt. This transforms point A to point B to make a new surface on the work and this process is repeated until the work-shape does not change appreciably between two successive steps and the equilibrium shape obtained.

This analogue method is approximate and cumbersome, its accuracy depend on the skill of the operator and is not advisable for use when a high degree of precision is desired.

4.4 Complex Variable Approach

Anode shape prediction in ECM has been attempted by employing the complex variables approach for the case of shaped workpieces and using simplified assumptions. It was reported that an equation was developed and used to determine IEG for both completely side insulated and bare and straight sides tools.

$$\frac{\text{Overcut at corner}}{\text{Machined gap}} = 1.159 \qquad (4.3)$$

However, a value of 1.7 was taken for this ratio, because it was assumed that the electrolyte conductivity and void fraction remains constant throughout. Conformal

mapping technique was used for the analysis of two-dimensional machining using straight-sided tools with a finite width. For an insulated tool it was assumed that the sides do not participate in metal removal. It was shown for a such a case that

$$0.731 \leq {}^{R_{oc}}/_{h} \leq 1.159 \qquad (4.4)$$

Where the lower limit applies to the case of a side insulated tool and the higher limit is for a bare tool. Use of mathematical models has not so far been generalized because workpieces have complex shapes and there are many parameters to consider.

4.5 Finite Element Method

In the view of the shortcomings in the above analytical models, Jain and Pandey [19] recommended the use of Finite element method (FEM) where the choice of the shape and size of the elements is convenient. It is easy to incorporate different boundary conditions and it is possible to analyze non-homogeneous situations. In this case, the effects of simultaneous variations in different parameters could easily be accounted and this method is explained in detail in Chapter 5.

CHAPTER 5

FINITE ELEMENT METHOD

5.1 Introduction

The Finite element method (FEM) is a numerical analysis technique for obtaining approximate solutions to a wide variety of engineering problems. Although it has been developed to study stresses in complex airframe structures, it is extended and applied to the broad field of continuum mechanics. Because of its diversity and flexibility as an analysis tool, it is receiving much attention in engineering problems and in industry. These applications range from deformation and stress analysis of automotive, aircraft, building, and bridge structures to field analysis of heat flux, fluid flow, magnetic flux, and other flow problems [39].

In this method a complex region (i.e., a continuum) is discretized into simple geometric shapes called finite elements. The material properties and the governing relationships are defined over these elements and expressed in terms of unknown values at element corners. An assembly process, duly considering the loading and constraints, results in a set of equations. Solution of these equations gives us the approximate behavior of continuum [7].

In more and more engineering situations today, it is necessary to obtain approximate numerical solutions to problems rather than exact closed-form solutions. Consider a example to find the load capacity of a plate that have several stiffeners and odd-shaped holes, the concentration of pollutants during non uniform atmospheric conditions, or the rate of fluid flow through a passage of arbitrary shape. We can write the governing equations and boundary conditions for these problems, but we see immediately that no simple analytical solution can be found. The difficulty in these three examples lies in the fact that either the geometry or some other feature of the problem is irregular or arbitrary. Analytical solutions to problems of this type seldom exist, yet these are the kinds of problems that engineers are called upon to solve.

The resourcefulness of the analyst usually comes to the rescue and provides several alternatives to overcome this kind of problems. One possibility is to make

simplifying assumptions to ignore the difficulties and reduce the problem to one that can be handled. Sometimes this procedure works but, more often it leads to serious inaccuracies or wrong answers. Now with the availability of computers, a more viable alternative is to retain the complexities of the problem and find an approximate numerical solution [17,39].

Several approximate numerical analysis methods have evolved over the years, a commonly used method is the finite difference method. The finite difference model of a problem gives a point wise approximation to the governing equations. This model (formed by writing difference equations for an array of grid points) can be improved by considering large number of points. With finite difference techniques we can face some fairly difficult problems for example, irregular geometries or an unusual specification of boundary conditions, at this situation the finite difference techniques become hard to use.

Unlike the finite difference method, which envisions the solution region as an array of grid points, the finite element method envisions the solution region as built up of many small, inter-connected sub regions or elements. A finite element model of a problem gives a piecewise approximation to the governing equations. The basic premise of the finite element method is that a solution region can be analytically modeled or approximated by replacing it with an assemblage of discrete elements. Since these elements can be put together in a variety of ways, they can be used to represent exceedingly complex shapes. Fig 5.1 shows how a finite difference model a finite element model can be used to represent a complex geometrical shape, such as cross-section of the turbine blade. For this we want to find the distribution of displacements and stresses for a given force loading or the distribution of temperature for a given thermal loading. The interior coolant passage of the blade, along with its exterior shape, gives it a non-simple geometry [39].

A uniform finite difference mesh would reasonably cover the blade (the solution region), but the boundaries must be approximated by a series of horizontal and vertical lines (or stair steps). On the other hand, the finite element model (using the simplest two-dimensional element e.g. the triangle) gives a better approximation to the region. Also, a better approximation to the boundary shape results because the curved boundary is represented by straight lines of any inclination. This example is not intended to suggest

that finite element models are decidedly better than finite difference models for all problems. The only purpose of the example is to demonstrate how the finite element method is particularly well suited for problems with complex geometries. Still another numerical analysis method is the boundary element method (boundary integral equation method). This method uses Green's theorem to reduce the dimensionality of the problem, a volume problem is reduced to a surface problem, and a surface problem is reduced to a line problem. The turbine blade cross section example would have no interior mesh, but rather a mesh of connected points along the exterior boundary and a mesh of connected points along the interior boundary. This method is computationally less efficient than finite elements and is not widely used in industry. It is popular for acoustic problems and is sometimes used as a hybrid method in conjunction with finite elements [17,39].

5.2 Working Procedure of Finite Element Method

In a continuum (i.e., a body of matter solid, liquid, gas or simply a region of space in which a particular phenomenon is occurring) problem of any dimension, the field variable whether it is pressure, temperature, displacement, stress, or some other quantity possesses infinitely many values because it is a function of each generic point in the body or solution region. Consequently, the problem is one with an infinite number of unknowns. [7]

The finite element discritization procedures reduce the problem to one of a finite number of unknowns by dividing the solution region into elements and by expressing the unknown field variable in terms of assumed approximating functions within each element. The approximating functions (sometimes called interpolation functions) are defined in terms of the values of the field variables at specified points called nodes or nodal points. Nodes usually lie on the element boundaries where adjacent elements are connected. In addition to boundary nodes, an element may also have a few interior nodes. The nodal values of the field variable and the interpolation functions for the elements completely define the behavior of the field variable within the elements.

For the finite element representation of a problem the nodal values of the field variable become the unknowns. Once these unknowns are found, the interpolation functions define the field variable throughout the assemblage of elements. Clearly, the nature of the solution and the degree of approximation depend not only on the size and

number of the elements used but also on the interpolation functions selected. As we cannot choose functions arbitrarily, because certain compatibility conditions should be satisfied. Often functions are chosen so that the field variable or its derivatives are continuous across adjoining element boundaries.

An important feature of the finite element method that sets it apart from other numerical methods is the ability to formulate solutions for individual elements before putting them together to represent the entire problem. For example, if we are treating a problem in stress analysis, we need the force–displacement or stiffness characteristics of each individual element and then assemble the elements to find the stiffness of the whole structure. In essence, a complex problem reduces to considering a series of greatly simplified problems.

Another advantage of the finite element method is the variety of ways in which one can formulate the properties of individual elements. There are basically three different approaches. The approach to obtaining element properties is called the *direct approach* because its origin is traceable to the direct stiffness method of structural analysis. Although the direct approach can be used only for relatively simple problems, because it is the easiest to understand when meeting the finite element method for the first time.

Element properties obtained by the direct approach can also be determined by the *variational approach.* The variational approach relies on the calculus of variations and involves extremizing a functional. For problems in solid mechanics the functional turns out to be the potential energy, the complementary energy, or some variant of these, such as the Reissner variational principle. Knowledge of the variational approach is necessary to work beyond the introductory level and to extend the finite element method to a wide variety of engineering problems. Where as the direct approach can be used to formulate element properties for only the simplest element shapes, the variational approach can be employed for both simple and sophisticated element shapes.

A third and even more versatile approach to deriving element properties is known as the *weighted residuals approach.* The weighted residuals approach begins with the governing equations of the problem and proceeds without relying on a variational statement. This approach is advantageous when it is possible to extend the finite element

method to problems where no functional is available. The method of weighted residuals is widely used to derive element properties for nonstructural applications such as heat transfer and fluid mechanics [17,31,32,39].

5.3 FEM Solution Procedure

Regardless of the approach used to find the element properties, the solution of a continuum problem by the finite element method [17,39] is given below:

1. Discretize the Continuum. The first step is to divide the continuum or solution region into elements. In Fig 4.1 the turbine blade has been divided into triangular elements that might be used to find the temperature distribution or stress distribution in the blade. A variety of element shapes may be used, and different element shapes can also be employed in the same solution region. When analyzing an elastic structure that has different types of components such as plates and beams, it is not only desirable but also necessary to use different elements in the same solution. Although the number and the type of elements in a given problem are matters of engineering judgment, the analyst can rely on the experience of others for guidelines.

2. Select Interpolation Functions. The next step is to assign nodes to each element and then choose the interpolation function to represent the variation of the field variable over the element. The field variable may be a scalar, a vector, or a higher-order tensor. Often, polynomials are selected as interpolation functions for the field variable because they are easy to integrate and differentiate. The degree of the polynomial chosen depends on the number of nodes assigned to the element, the nature and number of unknowns at each node, and certain continuity requirements imposed at the nodes and along the element boundaries. The magnitude of the field variable as well as the magnitude of its derivatives may be the unknowns at the nodes.

3. Find the Element Properties. Once the finite element model has been established (that is, once the elements and their interpolation functions have been selected), the matrix equations expressing the properties of the individual elements are determined by using any one of the three approaches: the direct approach, the variational approach, or the weighted residuals approach.

4. Assemble the Element Properties to Obtain the System Equations. To find the properties of the overall system modeled by the network of elements we must *assemble*

all the element properties. In other words, we combine the matrix equations expressing the behavior of the elements and form the matrix equations expressing the behavior of the entire system. The matrix equations for the system have the same form as the equations for an individual element except that they contain many more terms because they include all nodes. The basis for the assembly procedure stems from the fact that at a node, where elements are interconnected, the value of the field variable is the same for each element sharing that node. A unique feature of the finite element method is that the system equations are generated by assembly of the individual *element* equations. In contrast, in the finite difference method the system equations are generated by writing nodal equations.

5. Impose the Boundary Conditions. Before the system equations are ready for solution they must be modified to account for the boundary conditions of the problem. At this stage we impose known nodal values of the dependent variables or nodal loads.

6. Solve the System Equations. The assembly process gives a set of simultaneous equations that we solve to obtain the unknown nodal values of the problem. If the problem describes steady or equilibrium behavior, then we solve a set of linear or nonlinear algebraic equations. If the problem is unsteady, the nodal unknowns are a function of time, and we solve a set of linear or nonlinear ordinary differential equations.

7. Make Additional Computations If Desired. Many times we use the solution of the system equations to calculate other important parameters. For example, in a structural problem the nodal unknowns are displacement components. From these displacements we calculate element strains and stresses. Similarly, in a heat-conduction problem the nodal unknowns are temperatures, and from these we calculate element heat fluxes.

FEM is capable of analyzing all the three types of non-linear problems (i.e., materially non-linear, geometrically non-linear and both materially and geometrically non-linear) including problems with complex varying boundary conditions.

5.4 Variational Methods of Approximation

The variational methods of approximation include the Rayleigh-Ritz, Galerkin's, least squares, and collocation methods. All these methods find an approximate solution in the form of linear combinations of suitable approximation functions ϕ_j and undetermined parameters $c_j = \sum c_j \phi_j$. The parameters c_i are determined such that the

approximate solution satisfies the weighted - integral form or weak form of the governing equation or minimizes the quadratic functional associated with the equation. Various methods differ from each other in the choice of weight function (w) and approximate functions ϕ_j. The finite element method uses variational methods to formulate the discrete equations over an element [32].

5.4.1 The Rayleigh-Ritz Method

In the Rayleigh-Ritz method, the coefficients c_i of the approximation are determined using the weak form of the problem and the choice of weight functions is restricted to the approximate functions, $w = \phi_i$. The weak form contains both the governing differential equation and the natural boundary conditions of the problem, and it places less stringent continuity requirements on the approximate solution than the original differential equation or its weighted-integral form. The method is described below for a linear variational problem.

Consider the variational problem of finding the solution u such that

$$B(w,u) = t(w) \tag{5.1}$$

For all sufficiently differentiable functions w that satisfy the homogeneous form of any specified essential boundary conditions on u. when the functional B is bilinear and symmetric and t is linear, the problem of equation (5.1) is equivalent to minimization of the quadratic functional

$$I(u) = \frac{1}{2}B(u,u) - t(u) \tag{5.2}$$

The N- parameter Rayleigh – Ritz method solution for the problem is of the form

$$u_N = \sum_{j=1}^{N} c_j \phi_j \tag{5.3}$$

Where the constants c_j called the Ritz coefficients, are chosen such that equation (5.1) holds for $w = \phi_i (i = 1,2.....N)$.

For symmetric bilinear forms, the parameters in equation (5.3) are determined by minimizing the quadratic function given in equation (5.2).

$$\text{i.e., } \frac{\partial I}{\partial c_1} = 0, \frac{\partial I}{\partial c_2} = 0, ... \frac{\partial I}{\partial c_N} = 0 \tag{5.4}$$

5.4.2 The Galerkin's Method

In this method the choice of weight function ψ_i equal to the approximation function ϕ_i. The algebraic equations of the Galerkin's approximation are

$$\sum_{j=1}^{N} A_{ij} c_j = F_i \tag{5.5}$$

$$\text{where } A_{ij} = \int_{\Omega} \phi_i A(\phi_j)\,dx\,dy,\ F_i = \int_{\Omega} \phi_i [f - A(\phi_0)]\,dx\,dy \tag{5.6}$$

and A_{ij} is not symmetric.

The Galerkin's method is not the same as the Rayleigh-Ritz method. It should be clear that the former uses the weighted-integral form where as the latter uses the weak form to determine the coefficients of c_j and also the approximation functions used in the Galerkin's method are required to be of higher order than those used in the Rayleigh-Ritz method.

5.4.3 The Least Squares Method

In this method, we determine the parameters c_j by minimizing the integral of the square of the residual

$$\int_{\Omega} \frac{\partial R}{\partial c_i} R\,dx\,dy = 0 \tag{5.7}$$

$$\text{where } R = A\left(\sum_{j=1}^{N} c_j \phi_j + \phi_0\right) - f \neq 0 \text{ and A is a linear operator.}$$

$$\text{Then } \sum_{j=1}^{N} A_{ij} c_j = F_i \tag{5.8}$$

$$\text{where } A_{ij} = \int_{\Omega} A(\phi_i)\ A(\phi_j)\,dx,\ F_i = \int_{\Omega} A(\phi_i)[f - A(\phi_0)]\,dx$$

and here A_{ij} is symmetric, but it involves the same order of differentiation as in the governing equation.

5.4.4 The Collocation Method

In the collocation method, we want to find an approximate solution u_N to A (u) = f in the form of $u_N = \sum_{j=1}^{N} c_j \phi_j + \phi_0$ by requiring the residual in the equation to be identically zero at N selected points $X^i = (x^i, y^i)_{i=1,2,.....N}$ in the domain Ω.

$$R(x^i, y^i, c_j) = 0 \quad (i = 1,2,.....N) \tag{5.9}$$

The selection of the points X^i is crucial in obtaining a well-conditioned system of equations and ultimately in obtaining an accurate solution.

The final weighted – residual statement becomes

$$\int_{\Omega} \delta(X - X^i) R(X, c_j) dx\, dy = 0 \tag{5.10}$$

or $R(X^i, c_j) = 0$

Of all the above four described methods, Galerkin's method gives the solution very close to the exact solution compared with the other three variational methods [32].

5.5 Types of Elements and Their Choice

Over the last few years, different types of elements have been used in FEM and hence long list of alternative choice of elements exits. However, elements can be classified based on [23,31]

- Element shapes such as beam, bar, triangular, rectangular, tetrahedron, etc.
- Degrees of freedom.
- The completeness of displacement pattern conforming or non-conforming.
- The displacement model used linear, cubic, etc.
- The behavior of the elements plane stress, plane strain, axi-symmetric, etc.
- Nature of the problem one, two and three dimensional (Figs 4.2-4.4).

Selection of a particular type of element and the definition of an appropriate approximating function (i.e., interpolation function) is of utmost importance. Which element provides best alternative in practical usage is judged on the geometric forms of the problem, simplicity of formulation of element properties, versatility of application, computational efforts involved, accuracy obtainable, etc [23].

The size and shape of an element should be selected in such a way that it is capable of simulating accurately, the geometry of the problem. In two and three-dimensional analysis an alternative choice of the element is possible. For shapes involving curves which cannot be fitted exactly by triangular elements, *high order iso-parametric elements* are used to describe the geometry, which also reduces the number of elements to be used. So, four nodeded quadrilateral (rectangular) elements are better alternative to discritize the geometry [20].

Three-dimensional analysis of practical problems is expensive in terms of computation time and effort, in many cases it is simply not feasible. However, tetrahedron and Iso-parametric elements are more commonly employed under such conditions.

5.5 Range of Applications

Applications of the finite element method can be divided into three categories, depending on the nature of the problem to be solved. In the first category are the problems known as equilibrium problems or time-independent problems. The majority of applications of the finite element method fall into this category.

For the solution of equilibrium problems in the solid mechanics area, we need to find the displacement distribution and the stress distribution for a given mechanical or thermal loading. Similarly, for the solution of equilibrium problems in fluid mechanics, we need to find pressure, velocity, temperature, and density distributions under steady-state conditions.

In the second category are the so-called Eigen value problems of solid and fluid mechanics. These are steady-state problems whose solution often requires the determination of natural frequencies and modes of vibration of solid sand fluids. Examples of Eigen value problems involving both solid and fluid mechanics appear in civil engineering when the interaction of lakes and dams is considered and in aerospace engineering when the sloshing of liquid fuels inflexible tanks is involved. Another class of Eigen value problems includes the stability of structures and the stability of laminar flows.

In the third category is the multitude of time-dependent or propagation problems of continuum mechanics. This category is composed of the problems that result when the time dimension is added to the problems of the first two categories.

The range of possible applications of the finite element method extends to all engineering disciplines, but civil, mechanical, and aerospace engineers are the most frequent users of the method. In addition to structural analysis other areas of applications include heat transfer, fluid mechanics, electromagnetism, biomechanics, geomechanics, and acoustics. The method finds acceptance in multidisciplinary problems where there is a coupling between two or more of the disciplines. Examples include thermal structures where there is a natural coupling between heat transfer and displacements, as well as aero elasticity when there is a strong coupling between external flow and the distortion of the wing. [23,39]

5.6 Limitations of Finite Element Method

Finite element methods are extremely versatile and powerful and can enable engineers to obtain information about the behavior of complicated structures with almost any arbitrary loading. In spite of the significant advances that have been made in developing finite element packages, the results obtained must be carefully examined before they can be used.

The most significant limitation of finite element methods is that the accuracy of the obtained solution is usually a function of the mesh resolution. Any regions of highly concentrated stress, such as around loading points and supports, must be carefully analyzed with the use of a sufficiently refined mesh. In addition, there are some problems, which are inherently singular (the stresses are theoretically infinite). Special efforts must be made to analyze such problems.

An additional concern for any user is that because current packages can solve so many sophisticated problems, there is a strong temptation to "solve" problems without doing the hard work of thinking through them and understanding the underlying mechanics and physical applications. Modern finite element packages are powerful tools that have become increasingly indispensable to mechanical design and analysis. However, they also make it easy for users to make big mistakes.

Obtaining solutions with finite element methods often requires substantial amounts of computational time. Nevertheless, finite element packages have become increasingly indispensable to mechanical design and analysis. [17,23,39]

CHAPTER 6

MODELLING

ESD is a highly complex process. In fact, material removal rate in ESD is a non-linear problem involving a number of interacting parameters varying simultaneously within the inter-electrode gap. In this work, basically two types of models are proposed to study the interaction of various parameters during the process. These are

(i) Two- dimensional finite element model based on electric potential field by considering the effects of electrolyte concentration and temperature on electrolyte electrical conductivity and

(ii) One-dimensional analytical model based on electric potential by considering the effect of (a) void fraction and (b) void fraction and electrolyte temperature.

6.1 Finite Element Modelling

In ESD, when the charged electrolyte jet from nozzle (cathode) impinges on the surface of workpiece (anode), three flow regions are identified. These are: (1) Potential core region, (2) The stagnation region, and (3) Radial outward flow region (Fig. 6.1).

Following assumptions are made in developing the finite element model for electro stream drilling process.

1. The electrolyte jet coming from the glass nozzle strikes the work piece surface and then flows radially outwards.
2. The distribution of electrical potential varies linearly throughout the gap between the nozzle tip and workpiece.
3. The cross sectional area of the jet is constant in inter-electrode gap.
4. The work surface is flat initially.
5. The over-potential on the surfaces of the electrodes is negligible, therefore it is neglected.
6. Properties of the electrolyte are homogeneous.
7. Void fraction in the gap is neglected.

In ESD the thickness of diffusion layers at the electrodes is much smaller than the distance between the cathode and anode, the electrical potential (u), within the electrolyte space can be [22] described by

$$\text{div}(k\,\text{grad}\,u) = 0 \tag{6.1}$$

This is valid for determining u with boundary conditions and the distribution of electrical potential (u) between the electrodes is governed by Laplace's equation

$$\frac{\partial^2 u}{\partial x^2} + \frac{\partial^2 u}{\partial y^2} = 0 \tag{6.2}$$

The current density i_a at the work surface can be obtained by the gradient of the electrical potential (u) as

$$i_a = k\frac{\partial u}{\partial n^1} \tag{6.3}$$

Assuming the inter-electrode gap is represented by quadrilateral (Rectangular) elements (Fig 6.2), which continuously and uniquely represent the field variable u(x,y) in the solution domain and vary linearly with in the elements [7] , thus

$$u(x,y) = N_1u_1 + N_2u_2 + N_3u_3 + N_4u_4 = \left[N^e\right]\left(u^e\right) \tag{6.4}$$

where u^e is the column vector of nodal potentials for element e. The interpolation function N^e is defined as

$$N_i^e = \frac{1}{4}(1+\xi\xi_i)(1+\eta\eta_i) \tag{6.5}$$

where (ξ_i, η_i) are the coordinate of node i.

Galerkin's approach [7,32] was used to solve the equation (6.2).

$$\int_{\Omega}\Phi_i w_i dxdy = 0 \tag{6.6}$$

where w_i is the weighing function and ϕ_i is the residue.

$$\int\Phi_i\left[\frac{\partial^2 u}{\partial x^2} + \frac{\partial^2 u}{\partial y^2}\right]dxdy = 0$$

$$\iint\left[\frac{\partial}{\partial x}\left(\Phi\frac{\partial u}{\partial x}\right) + \frac{\partial}{\partial y}\left(\Phi\frac{\partial u}{\partial y}\right)\right]dA - \iint\left(\frac{\partial\Phi}{\partial x}\frac{\partial u}{\partial x} + \frac{\partial\Phi}{\partial y}\frac{\partial u}{\partial y}\right)dxdy = 0$$

$$\int_{\Gamma}\Phi\frac{\partial u}{\partial n}dS-\iint_{\Omega}\left(\frac{\partial\Phi}{\partial x}\frac{\partial u}{\partial x}+\frac{\partial\Phi}{\partial y}\frac{\partial u}{\partial y}\right)dxdy=0 \tag{6.7}$$

For quadrilateral elements, the coordinates x, y can also be represented in terms of nodal coordinates using the shape functions as given by equation (6.8).

$$\left.\begin{aligned}x&=N_1x_1+N_2x_2+N_3x_3+N_4x_4\\y&=N_1y_1+N_2y_2+N_3y_3+N_4y_4\end{aligned}\right\} \tag{6.8}$$

After expressing the derivatives of a function in (x,y) coordinates in terms of its derivatives in (ξ,η) coordinates, the stiffness matrix can be written as:

$$S_m^{\,e}=\int_{-1}^{1}\int_{-1}^{1}D^TD\left(u^e\right)\det J\,d\xi\,d\eta \tag{6.9}$$

where

$$\begin{aligned}D&=\begin{bmatrix}\frac{\partial N_1}{\partial x}&\frac{\partial N_2}{\partial x}&\frac{\partial N_3}{\partial x}&\frac{\partial N_4}{\partial x}\\\frac{\partial N_2}{\partial y}&\frac{\partial N_2}{\partial y}&\frac{\partial N_3}{\partial y}&\frac{\partial N4}{\partial y}\end{bmatrix}\\D&=\left[J^{-1}\right]\begin{bmatrix}\frac{\partial N_1}{\partial\xi}&\frac{\partial N_2}{\partial\xi}&\frac{\partial N_3}{\partial\xi}&\frac{\partial N_4}{\partial\xi}\\\frac{\partial N1}{\partial\eta}&\frac{\partial N_2}{\partial\eta}&\frac{\partial N_3}{\partial\eta}&\frac{\partial N_4}{\partial\eta}\end{bmatrix}\end{aligned} \tag{6.10}$$

and where J is the Jacobian matrix given by

$$J=\begin{bmatrix}\frac{\partial x}{\partial\xi}&\frac{\partial y}{\partial\xi}\\\frac{\partial x}{\partial\eta}&\frac{\partial y}{\partial\eta}\end{bmatrix} \tag{6.11}$$

The Gaussian quadrature approach [Appendix-4] together with equation (6.12) has been used to determine the coefficients of the stiffness matrix.

$$\int_{-1}^{1}\int_{-1}^{1}f(\xi,\eta)\,d\xi\,d\eta\approx w_1^2f(\xi_1,\eta_1)+w_2w_1f(\xi_2,\eta_1)+w_2^2f(\xi_2,\eta_2)+w_1w_2f(\xi_1,\eta_2) \tag{6.12}$$

where $w_1=w_2=1$

Further the solution of the first term i.e., the surface integral term in equation (6.6) can be evaluated by equation (6.13)

$$\int_{\Gamma}\phi\frac{\partial u}{\partial n'}ds=\int_{1}^{2}\phi_i\frac{\partial u}{\partial y}dx+\int_{2}^{3}\phi_i\frac{\partial u}{\partial x}dy-\int_{3}^{4}\phi_i\frac{\partial u}{\partial y}dx-\int_{4}^{1}\phi_i\frac{\partial u}{\partial x}dy \tag{6.13}$$

Further the equation (6.14) represents the assembled matrix for single element. In the same fashion, the assembly matrices for other elements can be obtained.

$$\begin{bmatrix} S_{ii} & S_{ij} & S_{ik} & S_{il} \\ S_{ji} & S_{jj} & S_{jk} & S_{jl} \\ S_{ki} & S_{kj} & S_{kk} & S_{kl} \\ S_{li} & S_{lj} & S_{lk} & S_{ll} \end{bmatrix} \begin{pmatrix} u_i \\ u_j \\ u_k \\ u_l \end{pmatrix} = 0 \tag{6.14}$$

Current density i_a can be evaluated by equation (6.3) on substituting the values of unknowns u's obtained from the assembled matrix [Appendix-3].

The boundary conditions

$u = 0$ at the nozzle tip, and

$u = E_v = V$ at the anode (workpiece)

have been used for obtaining the potentials at the nodes and thereafter the values of current densities have been evaluated and finally equation (6.15) has been used to determine the material removal rate of ESD process.

$$MRR = \eta\frac{E}{\rho_m}i_a \tag{6.15}$$

6.2 Radial Overcut

It was reported [19] that overcut for a partially bare tool the following empirical relationship holds:

$$R_{oc} = 2h + 0.1\left[6.283\left(r_c - 1\right)\right]^{0.5} \tag{6.16}$$

This equation yields inaccurate results especially at low feed rates, small corner radii of the tools or when equilibrium gap is large. An effort was made to correlate the radial overcut and equilibrium gap by applying regression technique based on 25 experimental points. This yields

$$R_{oc} = 0.1953h + 0.5779 \tag{6.17}$$

Equation (6.17) gives poor correlation when a generalized equation is to be derived involving a large number of points [19].

In the event of non-availability of any direct relationship between radial overcut and the parameters influencing it, the dimensional analysis of the parameters governing radial overcut has been carried out (Appendix-5). The derived formulation is expressed by equation (6.16).

$$\frac{R_{oc}}{D} = \alpha\left(\frac{u\,k}{f\sqrt{p}}\right)^{\beta} \tag{6.18}$$

where α and β are the constants whose values have been determined from the results of 20 experimental points [34].

6.3 Analytical Modelling

One-dimensional analytical modelling of Electrostream drilling process has been developed based on the following assumptions

1. In Electrostream drilling, the electrolyte flow is radially outward. So, it can be considered as one-dimensional.
2. The amount of dissolved metal is small, so that the flow contains only two phases namely, hydrogen gas and electrolyte.
3. The electrolyte is incompressible.
4. The over-potential on the surfaces of the electrodes is negligible and therefore can be neglected.
5. Specific heat with respect to temperature changes is neglected.
6. The electrolyte conductivity are linear is linearly dependent on temperature.

The distribution of electrical potential (u) along y-axis (Fig 6.1) is given by

$$\frac{\partial\left(k\frac{\partial u}{\partial y}\right)}{\partial y} = 0 \tag{6.19}$$

$$k\frac{\partial u}{\partial y} = C$$

$$k\frac{\partial u}{\partial y} = i_a \tag{6.20}$$

6.3.1 Considering the Effects of Void Fraction alone

By considering only the effects of void fraction on electrolyte conductivity, electrolyte conductivity can be expressed [24] as

$$k = k_o(1-\alpha_{vf})^m \tag{6.21}$$

Where m is a constant whose value is 1.5 for uniform void-distribution.

By substituting the equation (6.21) in equation (6.20), the current density is given by

$$k_o(1-\alpha_{vf})^m \frac{\partial u}{\partial y} = i_a \tag{6.22}$$

With boundary conditions

$u = 0$ at the nozzle tip (cathode)

$u = E_v = V$ at the workpiece (anode).

$$i_a = \frac{k_0(1-\alpha_{vf})^m V}{h} \tag{6.23}$$

The material removal rate of ESD can be computed using the following expression

$$MRR = \eta \frac{E}{\rho_w} i_a$$

$$MRR = \frac{Ek_0(1-\alpha_{vf})^m V}{\rho_w h} \tag{6.24}$$

6.3.2 Considering Effect of void Fraction and Electrolyte Temperature

The void fraction is the most important factor in determining the electrolyte conductivity and the shape of the workpiece [14]. So, by considering the effects of both electrolyte temperature and void fraction on electrolyte conductivity, electrolyte conductivity can be expressed [15] as

$$k = k_o(1-\alpha_{vf})^m[1+\alpha_t\theta] \tag{6.25}$$

$$\text{where } \alpha_{vf} = \frac{\delta}{1+\delta} \quad \text{and } \delta = \frac{IR_g(273+\theta+T_{0)}}{nFPQ_l} \tag{6.26}$$

Substituting the value of electrolyte conductivity (k) into equation (6.20), the current density is

$$k_o(1-\alpha_{vf})^m[1+\alpha_t\theta]\frac{\partial u}{\partial y} = i_a \tag{6.27}$$

with boundary conditions

$u = 0$ at the nozzle tip (cathode)

$u = E_v = V$ at the workpiece (anode).

In order to solve equation (6.27) with respect to conductivity changes, it is necessary to determine the increase in θ. Accounting for joule heating, the increase in θ may be determined from the energy balance, as

$$d(\rho_e v A C_p \theta) = A i_a du \tag{6.28}$$

Integrating the equation (6.28) and considering the boundary conditions $\theta(y=0)=0, u(y=0)=0$, the increase in temperature, θ is given by

$$\theta = \frac{i_a u}{C_p \sqrt{P \rho_e}} \tag{6.29}$$

Substituting the equation (6.29) into equation (6.25)

$$i_a = \frac{i_o}{1 - \left(\frac{\alpha_t i_o V}{C_p \sqrt{P \rho_e}} \right)} \tag{6.30}$$

where $i_o = \frac{k_o (1 - \alpha_{vf})^m V}{h}$

Maximum increase in temperature on the basis of equation (6.29) and equation (6.31) is given by

$$\theta_{max} = \frac{i_o V}{C_p \sqrt{P \rho_e} - \alpha_t i_o V} \tag{6.31}$$

Finally, the current density is given by the following expression

$$i_a = \frac{k_0 (1 - \alpha_{vf})^m V}{h} \left[1 + \frac{\alpha_t i_o V}{C_p \sqrt{P \rho_e} - \alpha_t i_o V} \right] \tag{6.32}$$

The material removal rate of ESD can be computed using the following expression

$$MRR = \eta \frac{E}{\rho_w} i_a = \frac{E k_0 (1 - \alpha_{vf})^m V}{\rho_w h} \left[1 + \frac{\alpha_t i_o V}{C_p \sqrt{P \rho_e} - \alpha_t i_o V} \right] \tag{6.33}$$

CHAPTER 7

RESULTS AND DISCUSSIONS

The modelling and analysis of the ESD process is carried out in two stages. In the first stage a two-dimensional FEM model was developed using Galerkin's approach. The inter-electrode gap is discritized by using the quadrilateral (rectangular) elements, which continuously and uniquely represent the filed variable i.e. electrical potential (u) in the solution domain and vary linearly with in the elements. By using the iso-parametric and Gauss quadrature approach the final assembly matrix [Appendix-3] for all the discritized elements has been obtained. The value of the electrical potential at different nodes has been determined from the final assembled matrix for further use in analyzing the process. The current density that is responsible for effecting the stock removal is determined by using equation (6.3).

In the second stage the analytical modelling of the process is carried out. In this part the effect of process parameters on material removal rate has been investigated by considering the effect of (a) electrolyte concentration (b) electrolyte conductivity (c) void fraction, and (d) void fraction and electrolyte temperature. The empirical relations for all these effects have been established [equations (6.24) and (6.33)]. The validation of the analytical results for the effect of electrolyte conductivity and electrolyte concentration has been performed by adapted experimental data [34]. In these two cases, the value of current density for estimating material removal rate and the value of electric potential for calculating the overcut were derived from the FEM model developed in stage one.

7.1 On Material Removal Rate (Considering the effect of electrolyte concentration)

7.1.1 Applied voltage

The analytical values of material removal rates are determined by considering the effect of electrolyte concentration by using equation (6.15). The value of electrolyte conductivity was experimentally determined for different electrolyte concentrations [34]. The obtained results at various input values of applied voltages for different electrolyte concentrations are given in Table 7.1. From Fig 7.1 it is clear that with the increase in applied voltage at different concentrations the material removal rate increases. It is

evident from Fig 7.1 that at high voltage 460V, material removal rate is nearly twice the one at low voltage i.e. 280 V. This is due to low dissolution efficiency at low voltage range because of long and narrow electrolytic path. At high voltage, the side machining on the return path of the electrolyte enhances the material removal rate.

7.2 Radial Overcut (Considering the effect of electrolyte concentration)

7.2.1 Effect of electrolyte concentration

Fig 7.2 shows the effect of electrolyte concentration on overcut. The analytical equation for overcut has been determined by using dimensional analysis [Appendix-5]. From Fig 7.2 it is clear that overcut increases with the increase in electrolyte concentration, this is inline with the equation (6.18), which shows that the radial overcut is proportional to the electrolyte concentration. The value of applied voltage used in equation (6.18) is determined from the FEM model.

7.2.2 Effect of nozzle diameter

From Fig 7.3 it is clear that the nozzle diameter has pronounced effect on radial overcut. The increase in nozzle diameter increases the radial overcut, this is inline with the equation (6.18).

7.2.3 Effect of feed rate

Fig 7.4 shows the effect of feed rate on radial overcut. Radial overcut decreases as the feed rate increases. This also satisfies the equation (6.18). The reason for this is the reduction in inter-electrode gap with higher tool feed rate. This also causes the increase in electrolyte flow rate. The increase in electrolyte flow rate reduces the time during which the electrolyte remains in contact with the hole sidewall on its outward flow and thus reducing the overcut.

7.2.4 Effect of pressure

With the increase of electrolyte pressure the radial overcut decreases. Fig 7.5 shows the relationship between the electrolyte pressure and analytical and experimentally obtained overcut. At low pressures machining time is more as compared to that at high pressures. So, the side machining on the return path of the electrolyte increases as the pressure of electrolyte decreases.

7.3 On Material Removal Rate (Considering the effect of electrolyte temperature)

7.3.1 Effect of applied voltage

An increase in applied voltage increases the material removal rate. Fig 7.6 shows the relation-ship between the applied voltage values and analytical and experimentally determined material removal rates. With the increase of applied voltage the temperature of electrolyte in the gap increases, and this effects the conductivity of the electrolyte and current supplied. From equation (6.15) it is also clear that material removal rate through electrolytic dissolution is proportional to the current supplied. This increases the material removal rate. The analytical results show a good approximation with the experimental results [34] as can be seen from Fig 7.6.

7.4 Radial Overcut (Considering the effect of electrolyte temperature)

7.4.1 Effect of voltage

With increase of applied voltage the radial overcut increases. Fig 7.7 shows the relationship between the applied voltage values and analytical and experimentally obtained radial overcut values. The value of radial overcut is more at the top surface of the workpiece. This may be due to the side machining of the hole by the electrolyte on its exit path causing increase in radial overcut.

7.42 Effect of nozzle diameter

An increase in nozzle diameter increases the radial overcut. From Fig 7.8 it is clear that the nozzle diameter has strong influence on radial overcut. This is inline with the equation (6.18). Any increase in nozzle diameter increases the current density within the gap and this results in corresponding increase in the side machining current which is responsible for increasing the overcut.

7.4.3 Effect of feed rate

Fig 7.9 shows the effect of feed rate on radial overcut. Radial overcut decreases by increasing the feed rate. This also satisfies the equation (6.18). At high feed rates the temperature and conductivity of electrolyte with in the gap decreases because of decrease in inter-electrode gap. This results in decrease in radial overcut.

7.4.4 Effect of pressure

With the increase of electrolyte pressure the radial overcut decreases. Fig 7.10 shows the relationship between the electrolyte pressure and analytical and experimentally obtained overcut. At low pressures machining time is more as compared with that at high pressures. So, the side machining on the return path of the electrolyte increases as the pressure of electrolyte decreases. With the increase of electrolyte pressure, the temperature rise with in the gap is reduced. So, this results in decrease in radial overcut.

7.5 On Material Removal Rate

7.5.1 Effect of inter-electrode gap (considering void fraction alone)

With the increase of inter-electrode gap (IEG) the material removal rate decreases. Fig 7.11 shows the relationship between the inter-electrode gap and analytical and experimentally obtained drilling rate at 460V. As the inter-electrode gap increases the current flowing with in the gap decreases. So, ultimately it effects the material removal rate, when void fraction is considered alone.

7.5.2 Effect of Inter-electrode gap (with void fraction and electrolyte temperature)

With the increase of inter-electrode gap (IEG) the material removal rate decreases. Fig 7.12 shows the relationship between the IEG with analytical and experimentally obtained material removal rate at 460 V. From equation (6.15) it is clear that when the gap increases the void fraction also increases. As the conductivity of the electrolyte is inversely proportional to the void fraction, the increase in void fraction reduces the conductivity which in turn results in reduced machining current in the gap thus resulting in reduced material removal rate.

7.5.3 Effect of electrolyte conductivity (with void fraction and electrolyte temperature)

An increase in electrolyte conductivity increases the material removal rate. Fig 7.13 shows the relationship between the electrolyte conductivity and analytical and experimentally obtained material removal rates at 460 V. As electrolyte conductivity increases, the current density in the gap increases thus resulting in increased MRR. From equation (6.15) it is clear that material removal rate in electrolytic action is proportional to the current supplied.

7.5.4 Effect of inter-electrode gap and electrolyte conductivity on MRR (With void fraction and electrolyte temperature)

The MRR decreases with the increase in inter-electrode gap. Fig 7.14 shows the relationship between the inter-electrode gap and analytical and experimentally obtained material removal rates at electrolyte conductivity 0.3808 (S/cm). The reason for this is the decrease in the current density in the gap which is responsible for material removal. Increasing in the inter-electrode gap also reduces the temperature and increases the void fraction, which results in reducing the conductivity of electrolyte. This reduces the MRR as current density is closely related to electrolyte conductivity.

CHAPTER 8

CONCLUSIONS AND SCOPE FOR FUTURE WORK

8.1 Conclusions

The following conclusions are drawn from the dissertation work:

1. Finite Element Method can be used for the analysis of Electrostream drilling process in predicting the material removal rate and radial overcut.
2. In FE modeling material removal rate is found to increase with the increase in applied voltage while considering the effects of different electrolyte concentrations and electrolyte temperatures on electrolyte conductivity.
3. The overcut during Electrostream drilling has been estimated by using dimensional analysis [Appendix-5].
4. Radial overcut increases with the increase in applied voltage, nozzle diameter and concentration, but it decreases with the increase in the feed rate and electrolyte pressure.
5. A one-dimensional analytical model is developed to study the effect of void fraction on material removal rate and electrolyte conductivity.
6. Material removal rate decreases with the increase in inter-electrode gap at different voltages.
7. The material removal rate has increased when void fraction considered alone, whereas the MRR is low when combined effects of void fraction and electrolyte temperature was taken into consideration.
8. The close correlation between the experimental data and proposed model results is achieved.

8.2 Scope for Future Work

The work embodied in this dissertation can be extended in the following directions:

1. A simulation model based on FEM can be developed for controlling the process in real time.

2. Three-dimensional FE modelling using higher order iso-parametric elements should be developed so as to compare the effectiveness of two-dimensional model.

1. Ahmed, M.S. and Duffield, A., "The drilling of small deep holes by acid ECM", *SME Technical paper,* 1990, MR90-243.

2. Anthony Newton, M., Machining, *Metals Hand book,* 9th edition, Vol.16, 1989, pp. 533-553.

3. Baker, G.E., "Hole drilling processes: experiences, applications, and selections", *Proceedings SME Nontraditional Machining Symposium,* Orlando, Florida, Amchem Company, 1991, pp. 1-12.

4. Bannard, J., "Fine hole drilling using electrochemical machining", *Proceedings of 19th International Machine Tool Design and Research Conference,* Manchester, 1978, pp. 503-510.

5. Bellows, G. and Kohls, J.B., "Drilling without drills", *American Machinist,* Special report 743, 1982, pp. 173-188.

6. Benedict, G.F., *Nontraditional Manufacturing Processes,* Marcel Dekker, Inc, New York, 1987.

7. Chandrupatla, T.R. and Belegundu, A.D., *Introduction to finite elements in Engineering,* Prentice-Hall of India, 2nd Edition, New Delhi, India, 2002.

8. Chang, C. S., Hourng, L.W. and Chung, C.T., "Tool design in electrochemical machining considering the effect of thermal-fluid properties", *Journal of Applied Electrochemistry,* Vol. 29, 1999, pp. 321-330.

9. Chrysolouris, G. and Wollowitz, M., "Electrochemical Hole Making", *Annals of CIRP,* Vol.33, No.1, 1984.

10. De Barr, A.E. and Oliver, D.A., *Electrochemical machining,* McDonald and Co. Ltd., 1975.

11. Gaikwad, K., Banait, N., Joshi, S.S. and Ramakrishan, N., "Modeling of micro-electrochemical machining (Micro-ECM) process", *Precision Engineering,* 2003, pp.180-187.

12. Ghosh, A. and Mallik, A.K., *Manufacturing Science,* Affiliated East-West Press Private Limited, New Delhi, 1985.

13. Hardisty, H., Mileham, A.R. and Shirvarni, H., "A finite element simulation of the electrochemical machining process, *Annals of CIRP,* Vol. 42, No.1, 1993, pp. 201-204.

14. Hocheng, H., Sun, Y.H., Lin, S.C. and Kao, P.S., "A material removal analysis of electrochemical machining using flat-end cathode" *Journal of Materials Processing Technology,* Vol.140, 2003, pp. 264–268.

15. Hourng, L.W. and Chang, C.S., "Numerical simulation of electrochemical drilling", *Journal of applied electrochemistry,* Vol. 23, 1993, pp. 316-321.

16. Hourng, L.W. and Chang, C.S., "Numerical simulation of two-dimensional fluid flow in electrochemical drilling", *Journal of applied electrochemistry,* Vol. 24, 1994, pp. 1170-1175.

17. Huebner, K.H.H., Dewhirst, D.L., Smith, D.E. and Byrom, T.G., *Finite Element Method,* Willey &sons, New York, 2001.

18. Jain, V.K., "An Analysis of ECM Process for Anode Shape Prediction", *Ph.D. Thesis,* University of Roorkee, Roorkee, India, 1980.

19. Jain, V.K. and Pandey, P.C., "Tooling design for ecm", *Precision Engineering,* 1980, pp. 195-206.

20. Jain, V.K. and Pandey, P.C., "Finite element approach to the two dimensional analysis of electrochemical machining", *Precision Engineering,* 1980, pp. 23-28.

21. Kozak, J., Budzynski, A.F. and Domanowski, P., "Computer simulation of electrochemical shaping (ECM-CNC) using a universal tool electrode", *Journal of Materials Processing Technology,* Vol. 76, 1998, pp. 161–164.

22. Kozak, J., Rajukar, K.P. and Balakrishna, R., "Study of electrochemical jet machining process", Transactions of ASME, *Journal of Manufacturing for Industry,* Vol. 118, 1996, pp. 490-498.

23. Martin, H.C. and Carey, G.F., *Introduction to the Finite element analysis,* Tata McGraw Hill Pub. Co. Ltd, 2nd Edition, New Delhi, 1977.

24. McCabe, W.L., Smith, J.C. and Harriott, P., *Unit operation of chemical engineering,* McGraw Hill Inc, 5th Edition, New York, 2002.

25. McGeough, J.A. and Baker M.B., "Electrochemical Machining Development and application", *ACS Symposium series 390,* 1989, pp. 578-580.

26. McGeough, J.A., *Principles of Electrochemical Machining,* Chapman and Hall, London, 1974.

27. Noot, M.J., Telesa, A.C., Jansen, J.K.M. and Mattheij, R.M.M., "Real time numerical simulation and visualization of electrochemical drilling", *Computing and Visualization in Science,* Vol.1, 1998, pp. 105-111.

28. Parker, S.P., *Fluid Mechanics Source Book,* McGraw Hill, New York.1987.

29. Rama Rao, S.V. and Mishra, P.K., "Hole Drilling by Electrojet", *Proceedings of the 5th international conference on production engineering Tokyo,* 1984, pp. 455-458.

30. Ruszaj, A. and Zybura-Skrabalak, M., "The mathematical modeling of electrochemical machining with flat ended universal electrodes", *Journal of Materials Processing Technology,* Vol.109, 2001, pp. 333- 338.

31. Rao, S.S., *The Finite Element Method in Engineering,* Butterworth-Heinemann Publications, 3rd Edition, New Delhi, 1999.

32. Reddy, J.N., *An Introduction to the Finite Element Method,* McGraw Hill Pub. Co. Ltd, New York, 1993.

33. Rourke, J.W. and Kennedy, D.C., "Electrochemical turning-a general purpose machine", *Proceeding 2nd International Conference on Development of Production Systems,* Copenhegan, Denmark, 27-31, 1973, pp. 161-172.

34. Sen, Mohan, "Study of Electro Jet Drilling in Some Super Alloys", Unpublished *Ph. D. Thesis,* Currently under Progress.

35. Sen, M. and Shan, H.S., "Comparative Study of small hole drilling in Nimonic C-263, *CD Proceeding 13th ISME Conference,* Roorkee, Paper No. PE-033.

36. Shan, H.S., *Advanced manufacturing processes,* Tata McGraw Hill, New Delhi, India (Under publication).

37. Wilson, J.F., *Theory and Practice of Electrochemical Machining,* John Willey and sons, London, 1988.

38. http://www.anotronic.co.uk

39. http://www.media.wiley.com

40. http://www.smarttec.co.uk

Papers published/ to be published from the present work

41. Sen, M., Amarendrakumar, B. and Shan, H.S., "Two dimensional finite element modeling of electro jet drilling process", *AIMTDR Conference,* Vellore, 2004 (Abstract accepted).

42. Sen, M., Amarendrakumar, B. and Shan, H.S., "Modelling of Electrochemical Jet Drilling Process using FEM", *International Conference on Manufacturing Automation,* Wuhan, China, 2004 (Abstract accepted).

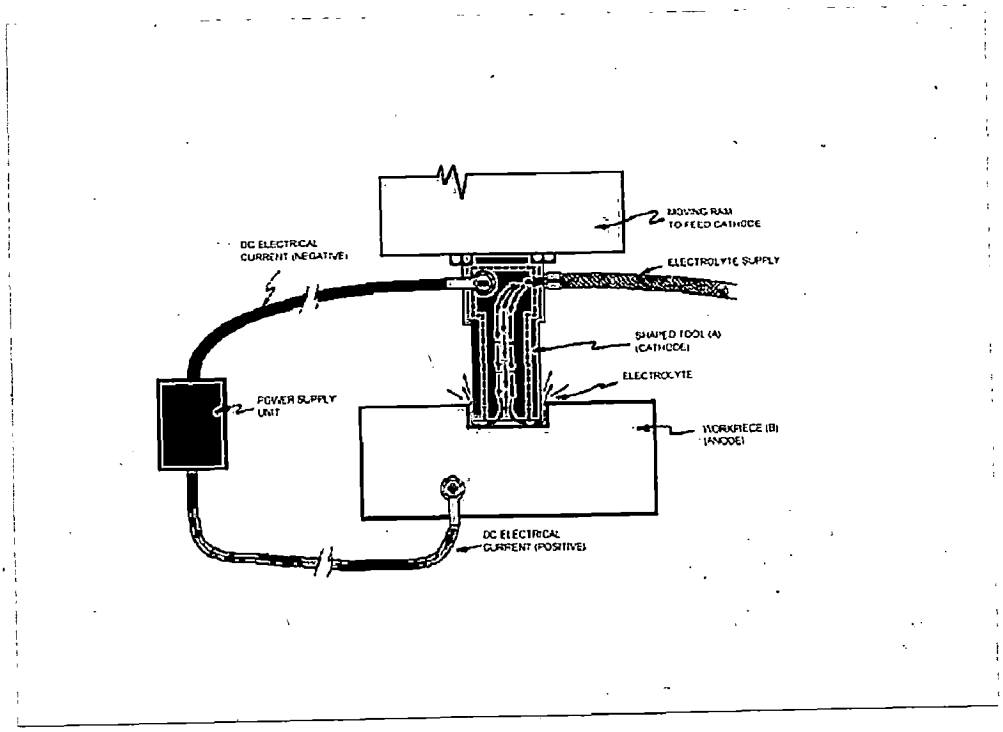

Fig 1.1 Schematic representation of electrochemical machining [38].

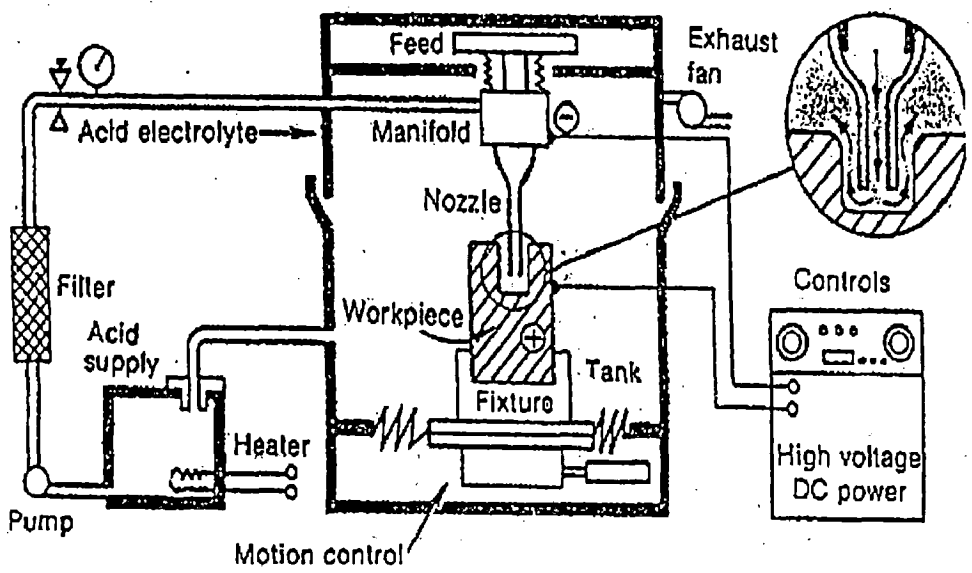

Fig 2.1 Schematic of material removal by Electrostream drilling process [2]

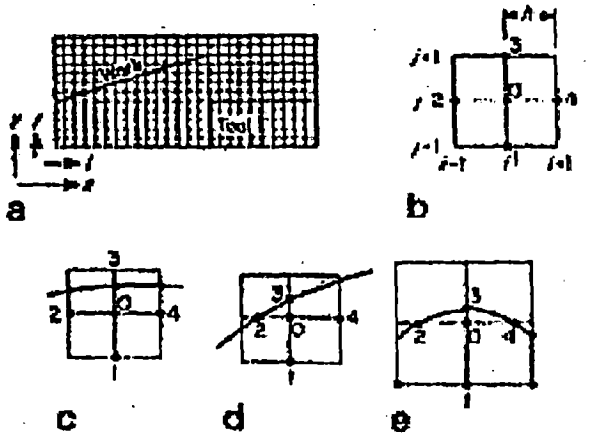

Fig 4.1 Finite difference analysis model of ECM process [19].
a). IEG-tool-work system discretised in square meshes b). A square mesh of spacing h having four equiplaced adjacent points 1,2,3,4 which from a regular star c). Boundary forms irregular star with one short from arm -03 d). Two short arms 02, 03 and e). Three short arms 02, 03, 04.

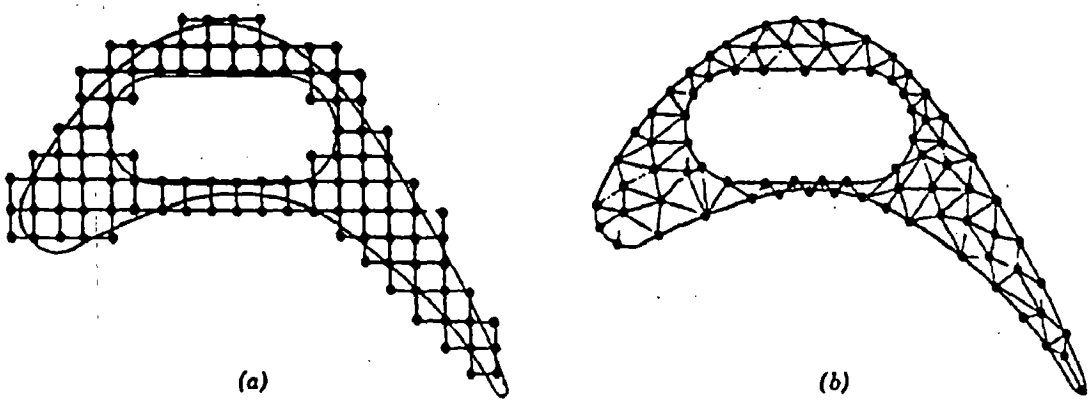

Fig 5.1 Discritization of turbine blade profiles for a) Finite difference and b) Finite element methods [32].

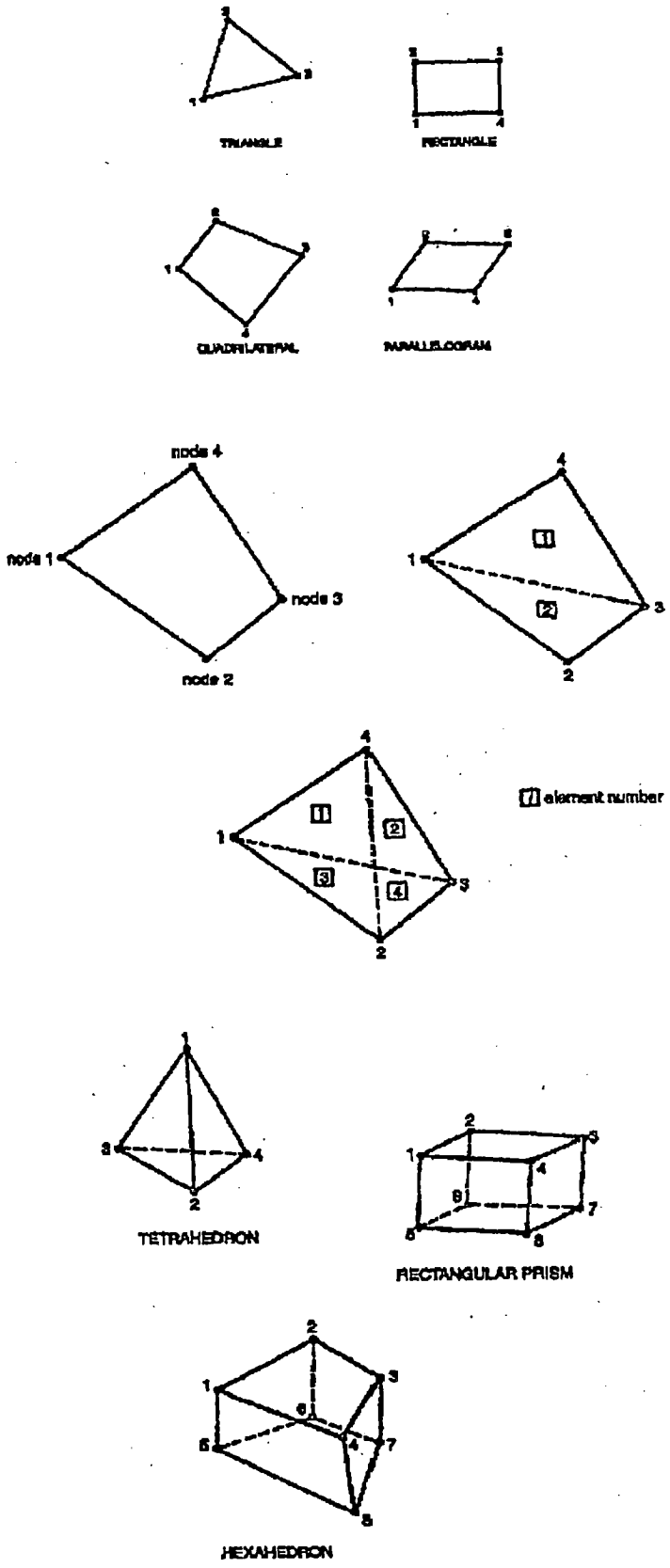

Fig 5.2 Two and three dimensional finite elements [37]

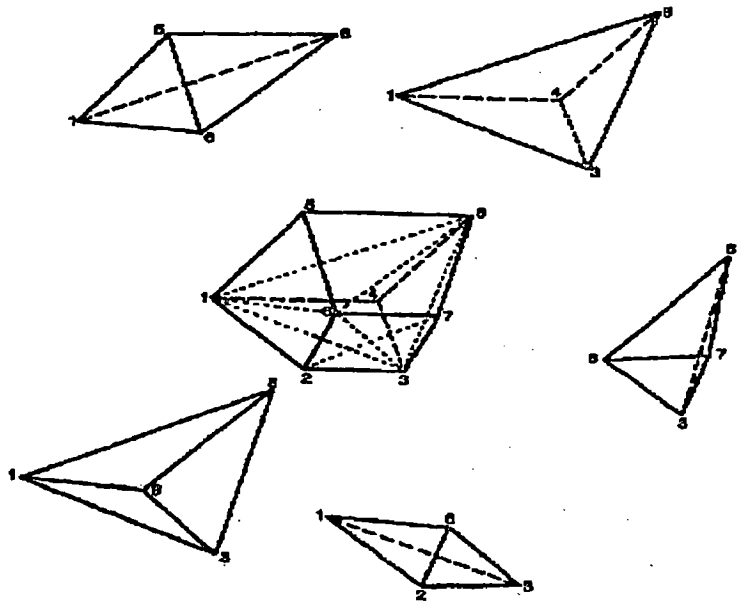

Fig 5.3 A hexahedron element as an assemblage of five tetrahedron elements [37]

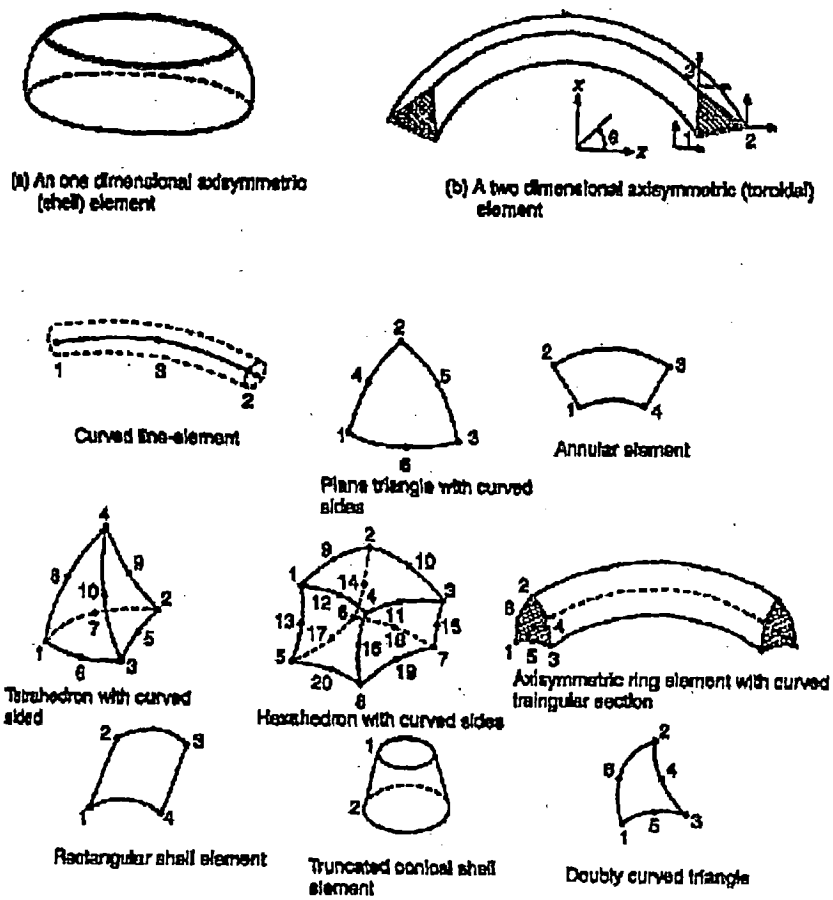

Fig 5.4 Finite elements with curved boundaries [37]

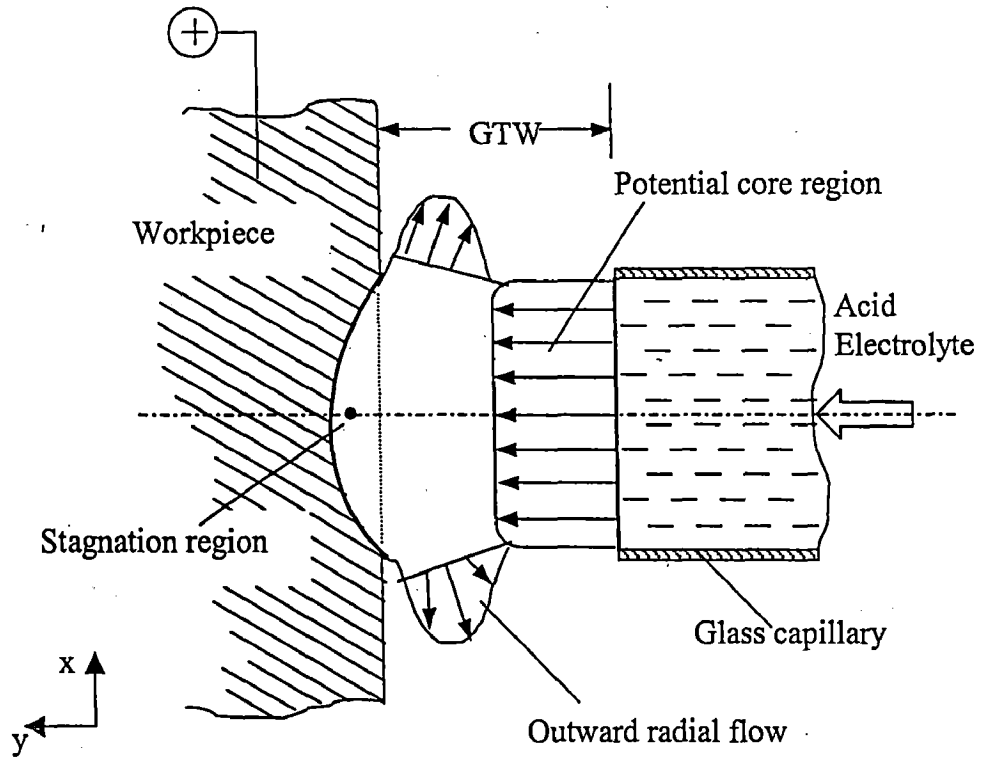

Fig 6.1 Schematic of principle of the Electrostream drilling

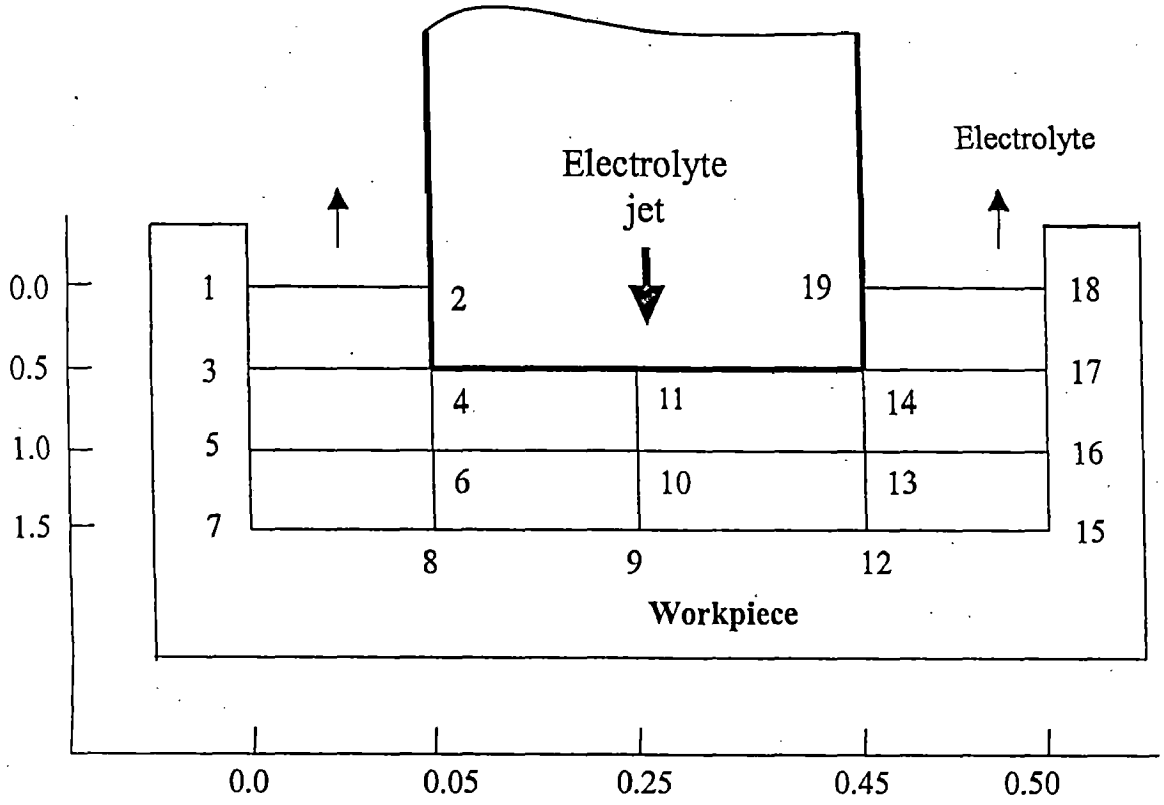

Fig 6.2 Finite element discritisation scheme used for the gap between capillary and workpiece in Electrostream drilling.

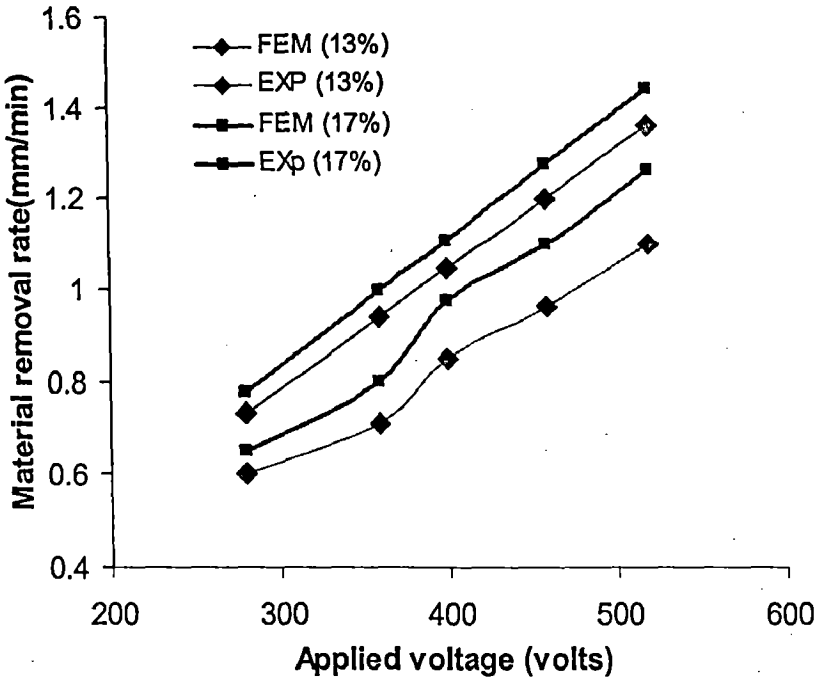

Fig 7.1 The effect of applied voltage on material removal rate for different electrolyte concentrations.

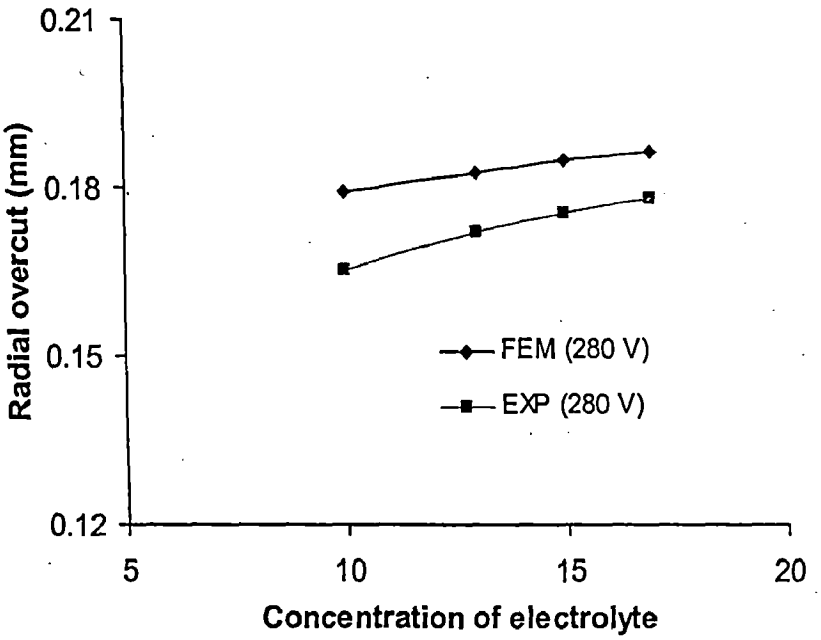

Fig 7.2 The effect of electrolyte concentration on radial overcut.

(Considering the effect of electrolyte concentration) — ??

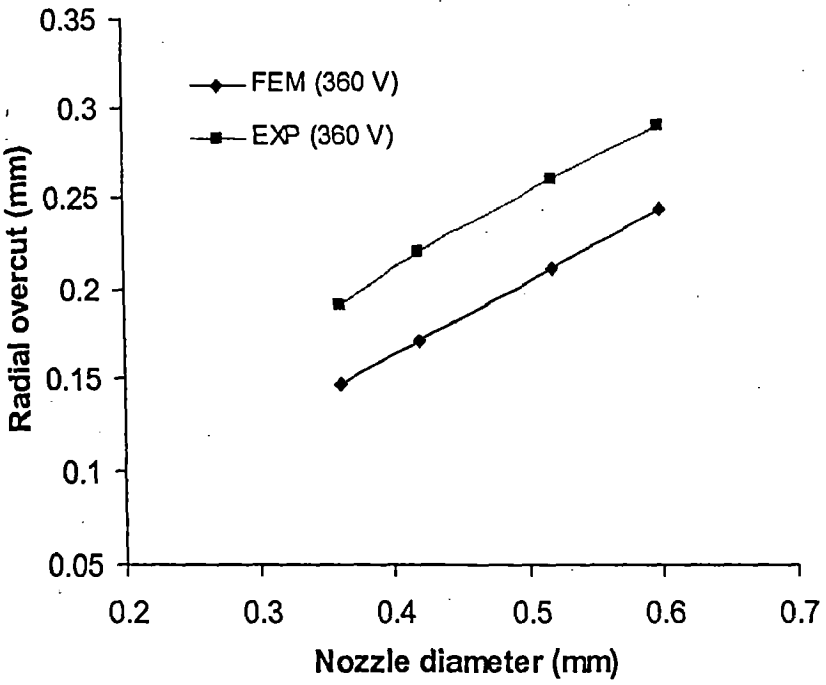

Fig 7.3 The effect of nozzle diameter on radial overcut.
(Considering the effect of electrolyte concentration)

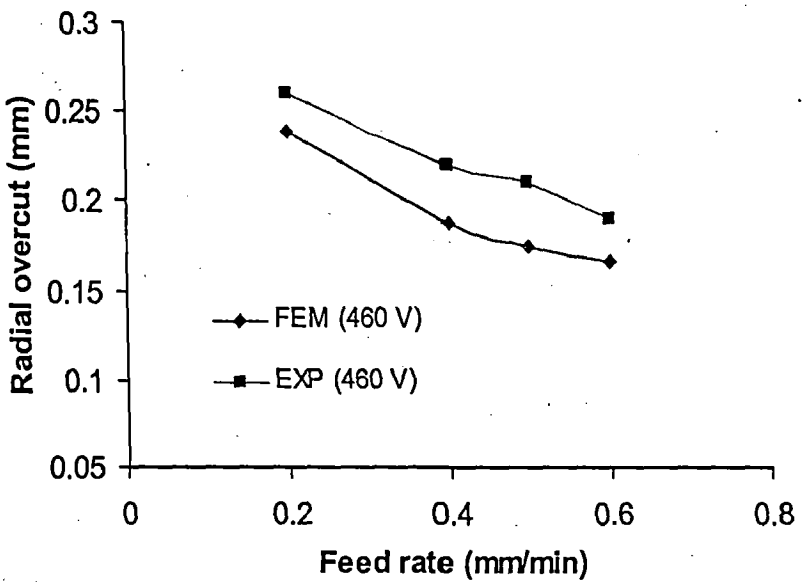

Fig. 7.4 The effect of feed rate on radial overcut.
(Considering the effect of electrolyte concentration)

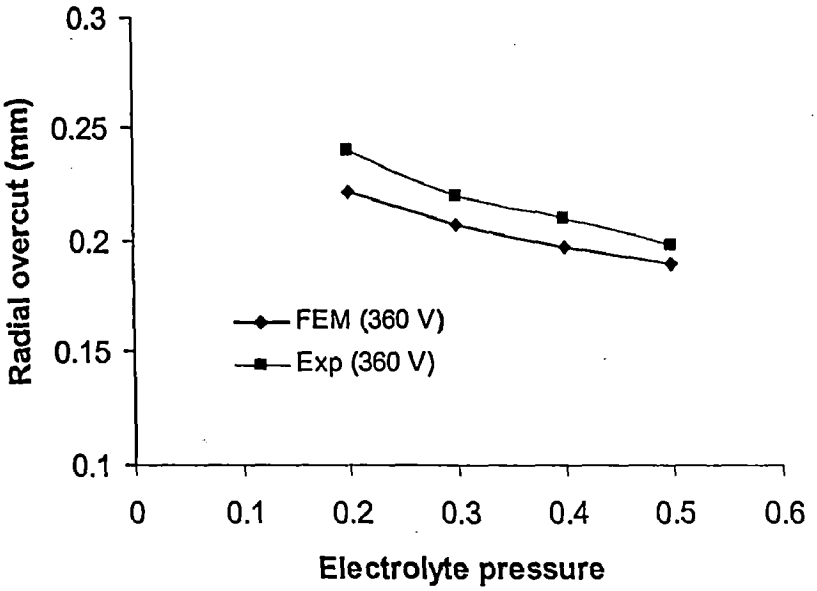

Fig. 7.5 The effect of electrolyte pressure on radial overcut
(Considering the effect of electrolyte concentration)

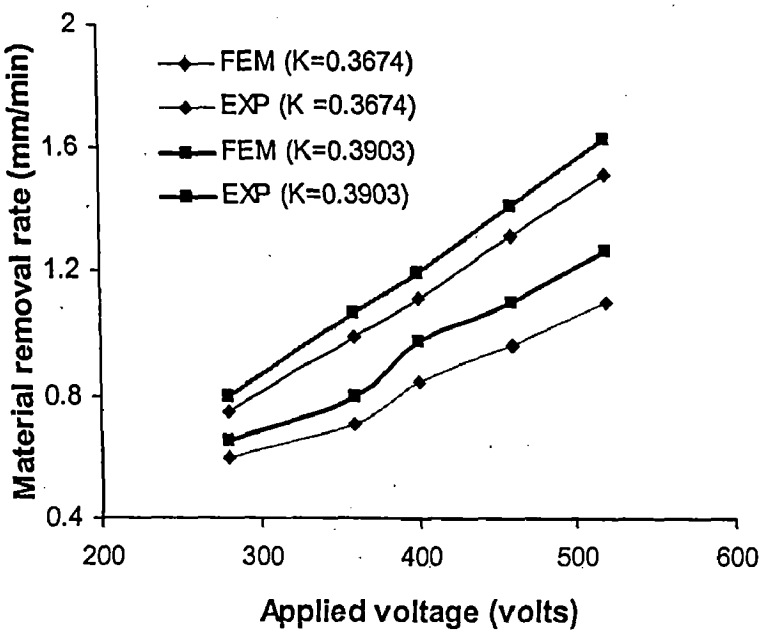

Fig 7.6 The effect of applied voltage on material removal rate for different electrolyte conductivities.

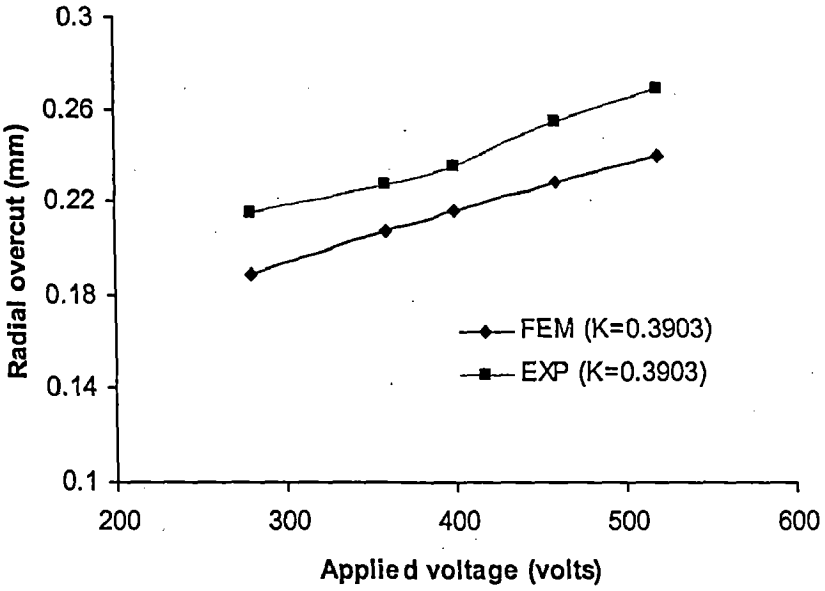

Fig 7.7 The effect of applied voltage on radial overcut
(Considering electrolyte temperature)

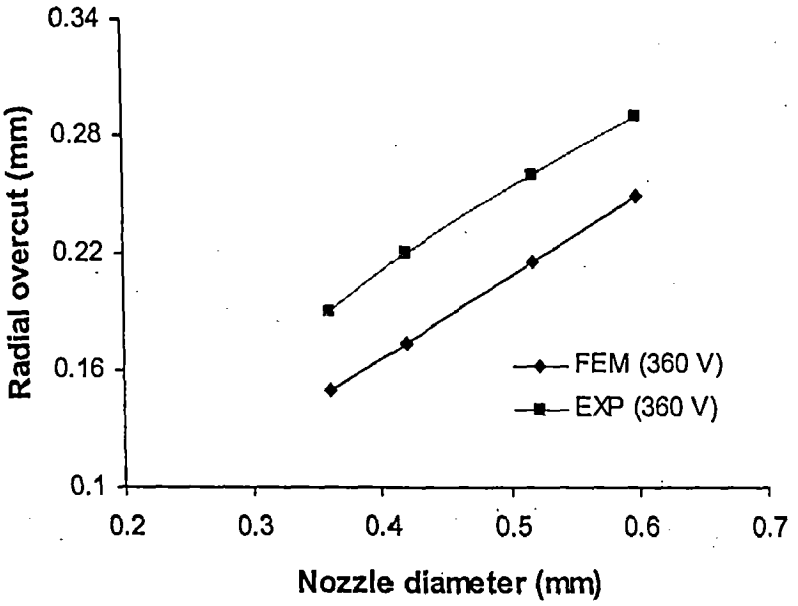

Fig 7.8 The effect of nozzle diameter on radial overcut
(Considering electrolyte temperature)

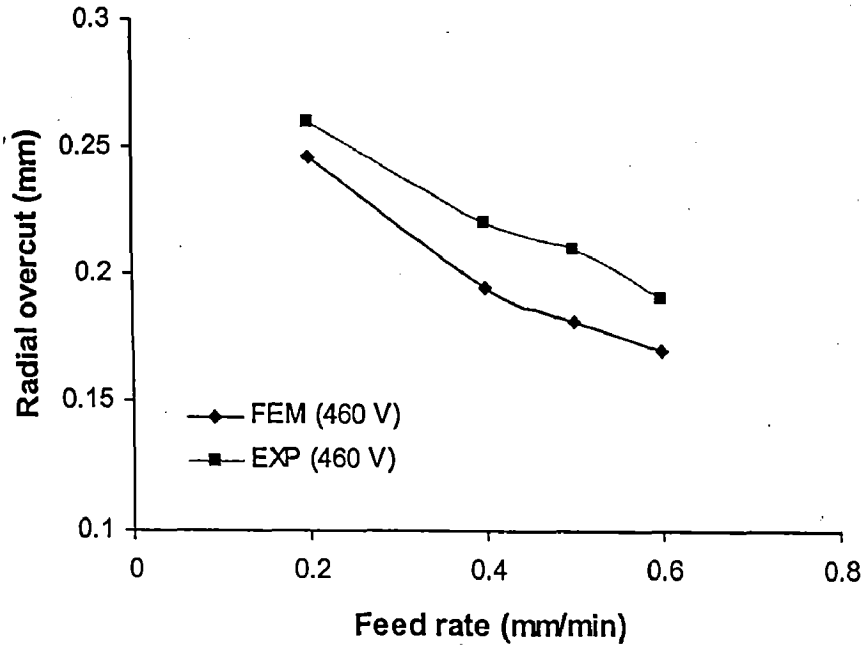

Fig 7.9 The effect of feed rate on radial overcut
(Considering electrolyte temperature)

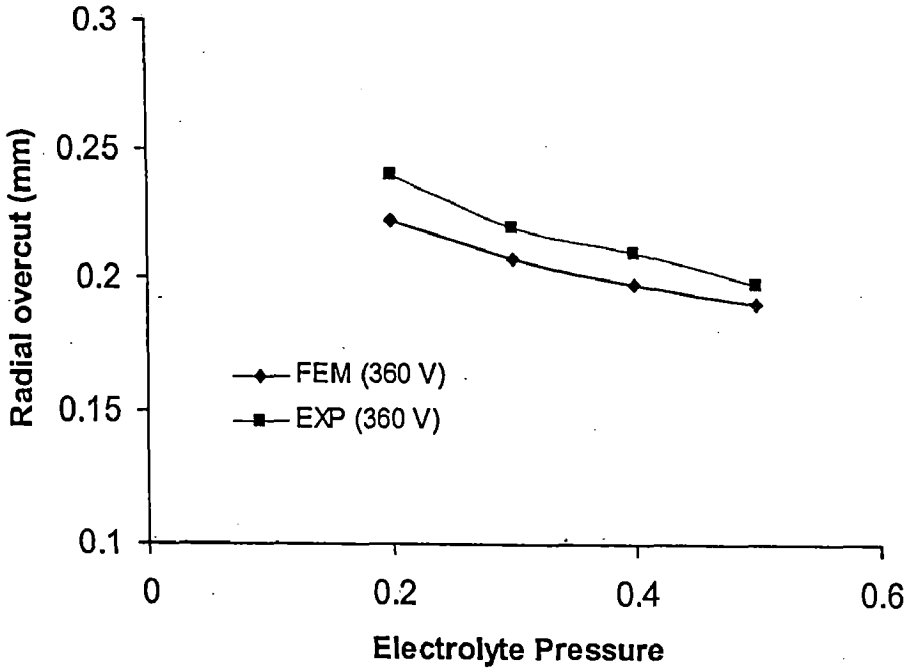

Fig 7.10 The effect of pressure of electrolyte on radial overcut
(Considering electrolyte temperature)

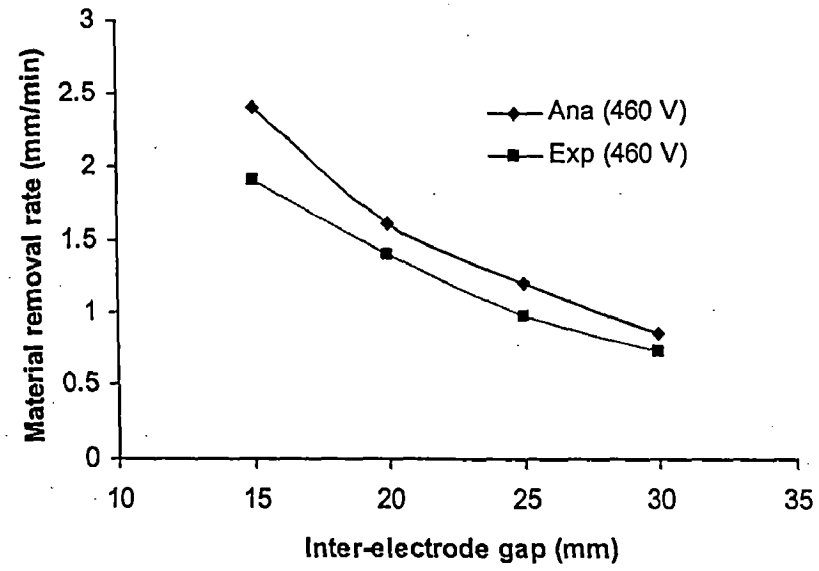

Fig 7.11 The effect of inter-electrode gap on material removal rate
(Considering void fraction alone)

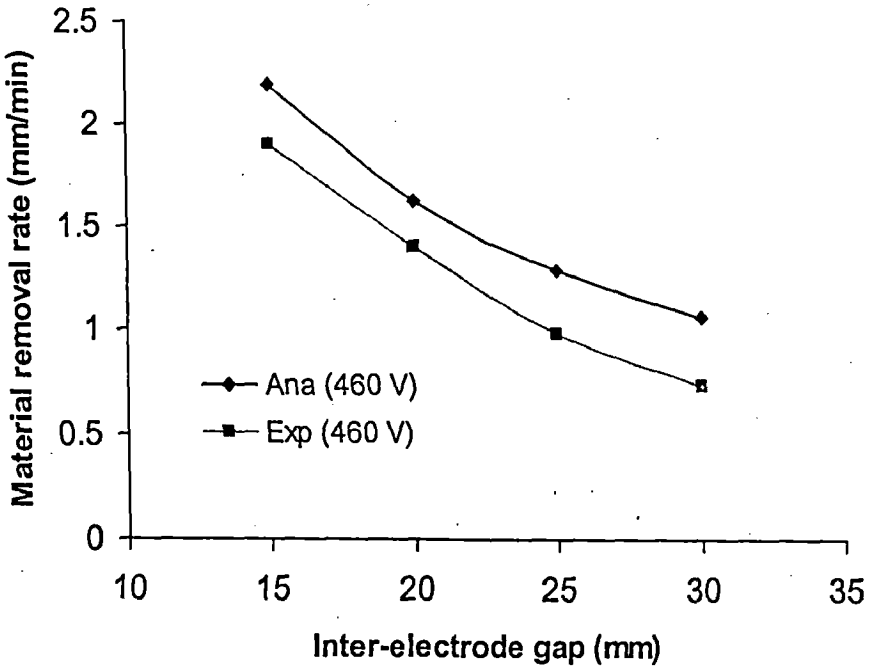

Fig 7.12 The effect of inter-electrode gap on material removal rate
(Considering void fraction and electrolyte temperature)

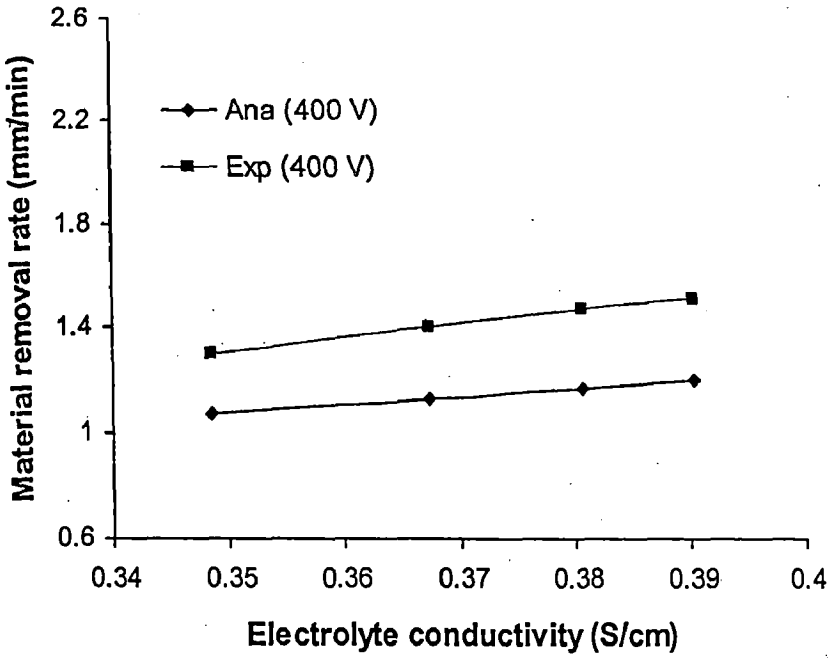

Fig 7.13 The effect of electrolyte conductivity on material removal rate (Considering void fraction and electrolyte temperature)

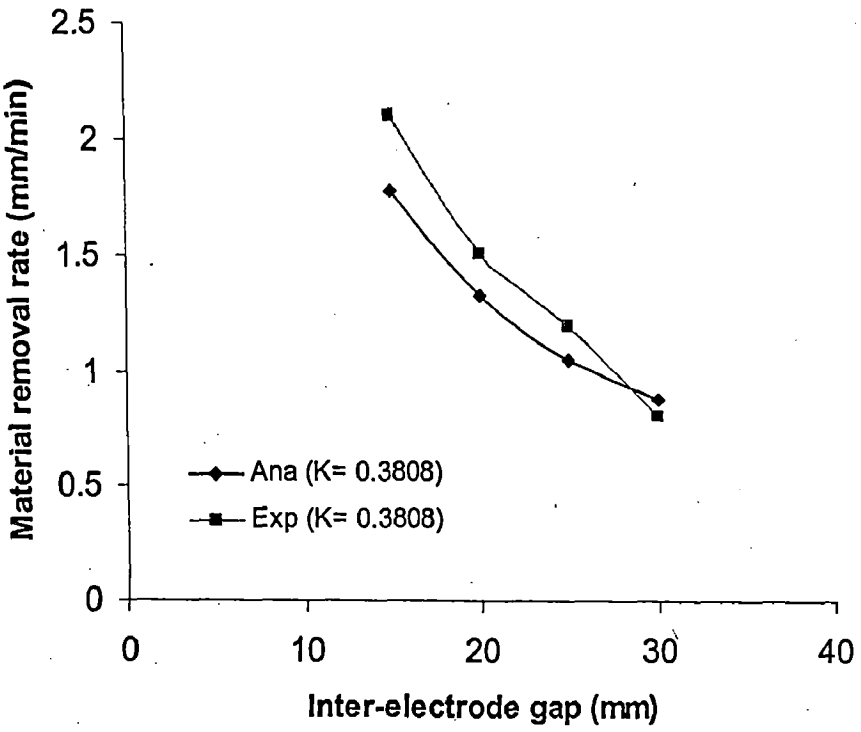

Fig 7.14 The effect of inter-electrode gap on material removal rate (Considering void fraction and electrolyte temperature).

Table1 Specifications for acid based Electrochemical-Drilling processes [40]

	STEM	CD	ESD	EJD
Min hole size (mm)	0.5	0.2	0.125	0.125
Max length /diameter	300	100	40	30
Hole tolerance (+/-mm)	0.03	0.03	0.03	0.05
Feed rate ($mm.min^{-1}$)	1-3.5	1-3.5	0.75-2.5	0

Table 2 The % composition in Nickel super alloy

Carbon	0.04-0.08
Silicon	0.40 max
Manganese	0.60 max
Sulfur	0.007 max
Silver	0.0005 max
Aluminum	0.60 max
Boron	0.005 max
Bismuth	0.0001 max
Cobalt	19.0-21.0
Chromium	19.0-21.0
Copper	0.20 max
Iron	0.7 max
Molybdenum	5.6-6.1
Lead	0.0020 max
Titanium	1.9-2.4
Aluminum and titanium	2.4-2.8
Nickel	Balance

$$\left(\frac{N}{n}\right)_{alloy} = \frac{\sum N_i x_{0i}}{\sum n_i x_{0i}} = 29.44$$

Table 3 Physical properties of Nickel super alloy

Density, g/cm^3 lb/in^3	8.360 0.302
Melting range Liquidus temperature °C Solidus temperature °C	 1355 1300
Specific heat , J/kg°C	461

Table 4 Thermal coefficient of electrical conductivity(α_t) and specific heat (C_p) for H_2SO_4 electrolyte [24].

Concentration of electrolyte (% vol basis)	α_t /k (%)	$C_p(J/kgk)$
5	0.960	4.129
10	1.082	4.081
13	1.142	4.053
15	1.182	4.034
17	1.223	4.016

Table 7.1 Theoretical (FE) material removal rate while considering the effect of concentration.

S. No	Applied Voltage (Volts)	Material removal rate (mm/min) at different concentrations			
		10%	13%	15%	17%
1	280	0.692	0.730	0.756	0.774
2	360	0.889	0.938	0.973	0.996
3	400	0.988	1.043	1.079	1.106
4	460	1.136	1.199	1.242	1.273
5	520	1.285	1.356	1.405	1.438

Inter-electrode gap = 25 mm, Feed rate = 0.25 mm/min, Nozzle diameter = 0.42mm, Pressure of electrolyte = 0.3 N/mm^2.

Table 7.2 Theoretical (FE) radial overcut while considering the effect of concentration.

S. No	Applied Voltage (Volts)	Radial Overcut (mm) at different concentrations			
		10%	13%	15%	17%
1	280	0.1793	0.1826	0.1847	0.1863
2	360	0.1953	0.1989	0.2012	0.2029
3	400	0.2024	0.2061	0.2086	0.2103
4	460	0.2122	0.2162	0.2187	0.2205
5	520	0.2213	0.2254	0.2280	0.2301

Inter-electrode gap = 25 mm, Feed Rate = 0.25 mm/min, Nozzle diameter = 0.50 mm, Pressure of electrolyte = 0.3 N/mm^2.

Table 7.3 Theoretical (FE) radial overcut while considering the effect of nozzle diameter (Considering electrolyte concentration).

S. No	Applied Voltage (Volts)	Radial Overcut (mm) at different nozzle diameter (mm)			
		0.36	0.42	0.52	0.60
1	280	0.1341	0.1565	0.1937	0.2235
2	360	0.1461	0.1704	0.2110	0.2435
3	400	0.1514	0.1766	0.2187	0.2523
4	460	0.1588	0.1852	0.2293	0.2646
5	520	0.1655	0.1931	0.2391	0.2759

Inter-electrode gap = 25 mm, Feed rate = 0.25 mm/min, electrolyte Concentration = 17%, Pressure of electrolyte = 0.3 N/mm^2

Table 7.4 Theoretical (FE) radial overcut while considering the effect of feed rate (Considering electrolyte concentration).

S. No	Applied Voltage (Volts)	Radial Overcut (mm) at different feed rates (mm/min)			
		0.20	0.40	0.50	0.60
1	280	0.2009	0.1588	0.1472	0.1388
2	360	0.2189	0.1729	0.1603	0.1506
3	400	0.2268	0.1792	0.1661	0.1561
4	460	0.2379	0.1879	0.1742	0.1637
5	520	0.2480	0.1959	0.1816	0.1707

Inter-electrode gap = 25 mm, Nozzle diameter = 0.50 mm, Concentration of electrolyte =17%, Pressure of electrolyte = 0.3 N/mm^2.

Table 7.5 Theoretical (FE) radial overcut while considering the effect of pressure of electrolyte (Considering electrolyte concentration).

S. No	Applied Voltage (Volts)	Radial Overcut (mm) at different electrolyte pressures (N/mm^2)			
		0.2	0.3	0.4	0.5
1	280	0.1995	0.1863	0.1774	0.1708
2	360	0.2174	0.2029	0.1932	0.1860
3	400	0.2253	0.2103	0.2002	0.1928
4	460	0.2362	0.2205	0.2099	0.2022
5	520	0.2463	0.2299	0.2189	0.2108

Inter-electrode gap = 25 mm, Feed rate = 0.25 mm/min, Nozzle diameter = 0.50 mm, Concentration of electrolyte =17% .

Table 7.6 Theoretical (FE) material removal rate while considering the effect of electrolyte conductivity.

S. No	Applied Voltage (Volts)	Material removal rate (mm/min) at different conductivities (S/cm)			
		0.3486	0.3674	0.3808	0.3903
1	280	0.707	0.746	0.772	0.799
2	360	0.938	0.991	1.029	1.065
3	400	1.053	1.114	1.156	1.196
4	460	1.236	1.308	1.359	1.407
5	520	1.425	1.509	1.569	1.626

IEG = 25 mm, Feed rate = 0.25 mm/min, Nozzle diameter = 0.50 mm, Pressure of electrolyte = 0.3 N/mm^2, Initial temperature of electrolyte = 27°C.

Table 7.7 Theoretical (FE) radial overcut while considering the effect of electrolyte conductivity.

S. No	Applied Voltage (Volts)	Radial Overcut (mm) at different conductivities (S/cm)			
		0.3486	0.3674	0.3808	0.3903
1	280	0.1806	0.1839	0.1862	0.1883
2	360	0.1988	0.2026	0.2052	0.2072
3	400	0.2068	0.2107	0.2135	0.2159
4	460	0.2183	0.2225	0.2255	0.2282
5	520	0.2291	0.2337	0.2368	0.2397

Inter-electrode gap = 25 mm, Feed rate = 0.25 mm/min, Nozzle diameter = 0.50 mm, Pressure of electrolyte = 0.3 N/mm^2, Initial temperature of electrolyte = 27°C

Table 7.8 Theoretical (FE) radial overcut while considering the effect of nozzle (Considering electrolyte temperature).

S. No	Applied Voltage (Volts)	Radial Overcut (mm) at different nozzle diameters (mm)			
		0.36	0.42	0.52	0.60
1	280	0.1355	.1581	0.1958	0.2259
2	360	0.1494	0.1743	0.2158	0.2490
3	400	0.1555	0.1810	0.2246	0.2591
4	460	0.1643	0.1917	0.2373	0.2738
5	520	0.1726	0.2014	0.2493	0.2876

Inter-electrode gap = 25 mm, Feed rate = 0.25 mm/min, Pressure of electrolyte = 0.3 N/mm^2, Initial temperature of electrolyte = 27°C, Concentration of electrolyte =17%.

Table 7.9 Theoretical (FE) radial overcut considering the effect of feed rate (Considering electrolyte temperature).

S. No	Applied Voltage (Volts)	Radial Overcut (mm) at different feed rates (mm/min)			
		0.20	0.40	0.50	0.60
1	280	0.2031	01605	0.1487	0.1398
2	360	0.2239	0.1768	0.1639	0.1541
3	400	0.2329	0.1841	0.1706	0.1604
4	460	0.2462	0.1945	0.1803	0.1694
5	520	0.2586	0.2043	0.1894	0.1779

Inter-electrode gap = 25 mm, Nozzle diameter = 0.50 mm, Pressure of electrolyte = 0.3 N/mm^2, Initial temperature of electrolyte = 27°C, Concentration of electrolyte =17%.

Table 7.10 Theoretical (FE) radial overcut while considering the effect of electrolyte pressure (Considering electrolyte temperature).

S. No	Applied Voltage (Volts)	Radial Overcut (mm) at different electrolyte pressures (N/mm^2)			
		0.2	0.3	0.4	0.5
1	280	0.2017	0.1883	0.1793	0.1726
2	360	0.2223	0.2075	0.1976	0.1903
3	400	0.2314	0.2159	0.2056	0.1979
4	460	0.2444	0.2282	0.2173	0.2092
5	520	0.2568	0.2397	0.2283	0.2197

Inter-electrode gap = 25 mm, Feed rate = 0.25 mm/min, Nozzle diameter = 0.50 mm, Initial temperature of electrolyte = 27°C, Concentration of electrolyte =17%.

Table 7.11 Analytical material removal rate while considering the effect of electrolyte pressure (Considering void fraction alone).

S. No	Applied Voltage (Volts)	Material removal rate (mm/min) at different IEGS (mm)			
		15	20	25	30
1	280	1.428	1.072	0.857	0.714
2	360	1.788	1.341	1.073	0.894
3	400	1.972	1.478	1.183	0.986
4	460	2.222	1.666	1.333	1.111
5	520	2.452	1.839	1.471	1.226

Pressure of electrolyte = 0.3 N/mm^2, Concentration of electrolyte = 15%, Flow rate = 0.3 lit/min, Specific heat C_p = 4.032 KJ/kg k, $\alpha_t = 0.01183/k$, Inlet temperature of electrolyte = 27°c, F = 96500 coulombs.

Table 7.12 Analytical material removal rate while considering the effect of IEG (Considering the void fraction and temperature effects).

S. No	Applied Voltage (Volts)	Material removal rate (mm/min) at different IEGS (mm)			
		15	20	25	30
1	280	1.403	1.046	0.834	0.694
2	360	1.755	1.304	1.038	0.862
3	400	1.941	1.439	1.144	0.949
4	460	2.189	1.618	1.284	1.064
5	520	2.410	1.776	1.406	1.163

Pressure of electrolyte = 0.3 N/mm^2, $\alpha_t = 0.01183/k$, Specific heat C_p = 4.032 KJ/kg k F = 96500 coulombs, Inlet temperature of electrolyte = 27°c, Flow rate = 0.3 lit/min, Concentration of electrolyte = 15%.

Table 7.13 Analytical material removal rate considering the effect of electrolyte conductivity.

S. No	Applied Voltage (Volts)	Material removal rate (mm/min) at different electrolyte conductivities (S/cm)			
		0.3486	0.3674	0.3808	0.3903
1	280	0.770	0.804	0.844	0.872
2	360	0.978	1.022	1.056	1.084
3	400	1.108	1.123	1.166	1.197
4	460	1.196	1.266	1.332	1.352
5	520	1.321	1.397	1.453	1.493

F = 96500 coulombs, Flow rate = 0.3 lit/min, Inlet temperature of electrolyte = 27°c, pressure of electrolyte = 0.3 N/mm^2

Table 7.14 Analytical material removal rate considering the effect of electrolyte conductivity

S. No	IEG (mm)	Material removal rate (mm/min) at different conductivities (S/cm)			
		0.3486	0.3674	0.3808	0.3903
1	15	1.624	1.718	1.785	1.834
2	20	1.209	1.278	1.327	1.363
3	25	0.963	1.017	1.055	1.084
4	30	0.799	0.845	0.876	0.903

F = 96500 coulombs, Flow rate = 0.3 lit/min, Applied voltage = 360 V, Inlet temperature of electrolyte = 27°c, Pressure of electrolyte = 0.3 N/mm^2.

The overall assembled matrix

$$\begin{bmatrix} 0.0324 & 0.0162 & -0.0162 & -0.0338 & 0 & 0 & 0 & 0 & 0 & 0 & 0 \\ -6.650 & 6.699 & 3.3210 & -3.3502 & 0 & 0 & 0 & 0 & 0 & 0 & 0 \\ -3.3210 & -3.350 & 4.7015 & -6.649 & 0.0346 & -2.7098 & 0 & 0 & 0 & 0 & 0 \\ 0 & 0 & -3.288 & 4.335 & -1.6332 & 2.1664 & 0 & 0 & 0 & 2.2436 & 0 \\ 0 & 0 & -1.6832 & 1.6332 & 5.0014 & -3.2843 & -0.0329 & -0.0671 & 0 & 0 & 0 \\ 0 & 0 & -0.0338 & -0.5659 & -3.2843 & 5.7399 & 1.6990 & -2.8109 & 0.1201 & -1.398 & 0 \\ 0 & 0 & 0 & 0 & -1.6832 & -1.6442 & 3.0183 & 0.0324 & 0 & 0 & 0 \\ 0 & 0 & 0 & 0 & -0.0338 & -0.4984 & 0.0160 & 1.0050 & -0.7992 & 0.2834 & 0 \\ 0 & 0 & 0 & 0 & 0 & 0.2834 & 0 & -0.7666 & 0.9667 & -0.4832 & 0 \\ 0 & 0 & 0 & 0.1201 & 0 & -1.698 & 0 & 0.1201 & -0.6535 & 2.201 & 0 \\ 0 & 0 & 0 & -0.7660 & 0 & 0.4989 & 0 & 0 & 0 & -0.4832 & 0.9667 \end{bmatrix} \begin{bmatrix} u_1 \\ u_2 \\ u_3 \\ u_4 \\ u_5 \\ u_6 \\ u_7 \\ u_8 \\ u_9 \\ u_{10} \\ u_{11} \end{bmatrix} = 0$$

With boundary conditions $u_2 = u_4 = u_{11} = 0$, $u_7 = u_8 = u_9 = V$ then,

$u_1 = 0.408V$	$u_3 = 0.817V$	$u_5 = 0.905V$	$u_6 = 0.929V$	$u_{10} = 0.959V$

Gauss Quadrature Method For two point

For two – point gauss approximation

$$\int_{-1}^{1} f(\xi)\,d\xi = w_1 f(\xi_1) + w_2 f(\xi_2) \qquad \text{(A. 2.1)}$$

where w_1, w_2 are the weights and ξ_1, ξ_2 are the sampling points or Gauss points. We assume a cubic polynomial for above Eq (A. 2.1) to be exact. Then

$$f(\xi) = c_1\xi^3 + c_2\xi^2 + c_3\xi + c_4$$

$$\text{Error} = \int_{-1}^{1} (c_1\xi^3 + c_2\xi^2 + c_3\xi + c_4)\,d\xi - [w_1 f(\xi_1) + w_2 f(\xi_2)] \qquad \text{(A. 2.2)}$$

Requiring zero error yields

$$\begin{aligned} w_1 + w_2 &= 2 \\ w_1\xi_1 + w_2\xi_2 &= 0 \\ w_1\xi_1^2 + w_2\xi_2^2 &= \frac{2}{3} \\ w_1\xi_1^3 + w_2\xi_2^3 &= 0 \end{aligned} \qquad \text{(A. 2.3)}$$

The unique solution of these nonlinear equations is

$$\begin{aligned} w_1 &= w_2 = 1 \\ -\xi_1 &= \xi_2 = 1/\sqrt{3} = 0.577350 \end{aligned} \qquad \text{(A. 2.4)}$$

The above method is extended to two-dimensional integrals, and then it is of the form

$$\int_{-1}^{1}\int_{-1}^{1} f(\xi,\eta)\,d\xi\,d\eta \approx w_1^2 f(\xi_1,\eta_1) + w_2 w_1 f(\xi_2,\eta_1) + w_2^2 f(\xi_2,\eta_2) + w_1 w_2 f(\xi_1,\eta_2) \qquad \text{(A. 2.5)}$$

where $w_1 = w_2 = 1, \xi_1 = \eta_1 = -0.577350$ and $\xi_2 = \eta_2 = 0.577350$

This method often finds its usage in solving element stiffness for a quadrilateral element and high order elements.

Analysis of overcut in ESD process

Due to low correlation coefficient obtained during regression analysis dimensional analysis was performed to obtain a relationship between the overcut (R_{oc}) and the variables that govern its magnitude. The parameters considered for this and their dimension are shown below.

Electrical potential (u)	$M^{\frac{1}{2}}L^{\frac{1}{2}}T^{-1}$
Conductivity of electrolyte (K)	T^{-1}
Pressure of electrolyte (P)	$ML^{-1}T^{-2}$
Diameter of nozzle (D)	L
Feed rate (f)	LT^{-1}

Buckingham's π theorem is used for determining the dimensionless groups π_1, π_2, π_3 corresponding to the variables. They are

$$\pi_1 = D^{a_1} K^{b_1} P^{c_1} R_{oc} \quad \text{(A. 5.1)}$$

$$\pi_2 = D^{a_2} K^{b_2} P^{c_2} u \quad \text{(A. 5.2)}$$

$$\pi_3 = D^{a_3} K^{b_3} P^{c_3} f \quad \text{(A. 5.3)}$$

Solving for $a_1, a_2, a_3, b_1, b_2, b_3, c_1, c_2, c_3$ leads to following relationships

$$\pi_1 = \frac{R_{oc}}{D} \quad \text{(A. 5.4)}$$

$$\pi_2 = \frac{u}{D\sqrt{P}} \quad \text{(A. 5.5)}$$

$$\pi_3 = \frac{f}{DK} \quad \text{(A. 5.6)}$$

Substituting the values of π_1, π_2, π_3 , we get

$$f_1\left(\frac{R_{oc}}{D}, \frac{u}{K\sqrt{P}}, \frac{f}{DK}\right) = 0$$

$$\frac{R_{oc}}{D} = f_2\left(\frac{u}{D\sqrt{p}}, \frac{f}{DK}\right) \qquad \text{(A. 5.7)}$$

From the power law the following equation has been obtained.

$$\frac{R_{oc}}{D} = \alpha\left(\frac{uK}{f\sqrt{p}}\right)^{\beta} \qquad \text{(A. 5.8)}$$

Where α, β are the constants whose values have been obtained from the results of 20 experimental points.